INSTITUTE OF PHYSICS PUBLISHING REPORTS ON PROGRESS IN PHYSICS

Rep. Prog. Phys. **65** (2002) 895–954 PII: S0034-4885(02)31132-1

Wavefronts in time-delayed reaction–diffusion systems. Theory and comparison to experiment

Joaquim Fort[1] **and Vicenç Méndez**[2]

[1] Departament de Física, Universitat de Girona, Campus de Montilivi, 17071 Girona, Catalonia, Spain
[2] Facultat de Ciències de la Salut, Universitat Internacional de Catalunya, Gomera s/n, 08190 Sant Cugat del Vallès, Catalonia, Spain

E-mail: joaquim.fort@udg.es and vmendez@csc.unica.edu

Received 22 November 2001, in final form 23 April 2002
Published 14 May 2002
Online at stacks.iop.org/RoPP/65/895

Abstract

We review the recent theoretical progress in the formulation and solution of the front speed problem for time-delayed reaction–diffusion systems. Most of the review is focused on hyperbolic equations. They have been widely used in recent years, because they allow for analytical solutions and yield a realistic description of some relevant phenomena. The theoretical methods are applied to a range of applications, including population dynamics, forest fire models, bistable systems and combustion wavefronts. We also present a detailed account of successful predictions of the models, as assessed by comparison to experimental data for some biophysical systems, without making use of any free parameters. Areas where the work reviewed may contribute to future progress are discussed.

Contents

1. Introduction

Wavefronts are ubiquitous in Nature. Some physical examples are combustion flames, superconducting, crystallization and solidification fronts. Some biological examples are the invasions of biological populations, the waves of advance of advantageous genes, the growth of virus plaques and of cancer tumours, the propagation of epidemics, etc.

Wavefronts are special solutions to the dynamics of systems with several equilibrium states. Wavefronts (or fronts for short) are usually defined as solutions such that they travel with constant shape and connect an unstable (initial) and a stable (final) state. In practice, this means simply that before the propagation of the front the system is in an unstable state, and after the front has swept along the system, its state is stable. The relevant variable depends on the system and process one wishes to describe. For example, in range expansions of biological populations a relevant variable is the population density. In the propagation of some flames, this role is played by the temperature, etc.

The simplest, most well-known system with wavefront solutions can be introduced as follows. Let n stand for the number density of a chemical or biological species. We will consider, for the time being, the very simple case of a one-dimensional (1D) system (e.g. we may consider a chemical species in a very thin wire, or a biological species living along a coast). Then, n is the number of particles or individuals per unit length. According to Fick's law, the diffusion flux (measured in number of particles or individuals that cross a point of the 1D system per unit time) is

$$J = -D\frac{\partial n}{\partial s}, \tag{1}$$

where s is the space coordinate and D is the diffusion coefficient. On the other hand, the mass balance equation reads

$$\frac{\partial n}{\partial t} = -\frac{\partial J}{\partial s} + F(n), \tag{2}$$

where $F(n)$ is the net number of particles (or individuals) that appear per unit time and length (recall that we are dealing with 1D systems for the moment), and t is the time. The interpretation of this equation is straightforward: integrating it over a subsystem of length L, we obtain simply that the net change of particles (individuals) is equal to the net number appearing per unit time because of the reactive (reproductive) process, minus the net number leaving the system per unit time. Combining the previous two equations yields

$$\frac{\partial n}{\partial t} = D\frac{\partial^2 n}{\partial s^2} + F(n), \tag{3}$$

which is the simplest possible equation with wavefront solutions. This equation has been applied to the spread of advantageous genes [1], combustion flames [2], dispersions of biological populations [3], epidemic models [4], etc.

The mass balance equation (2) is untouchable in the present context, because of the interpretation we have presented below it. Its status is in sharp contrast to that of equation (1), which is only an approximation to physical reality. It is a linear relation between cause (a nonhomogeneous density, $\partial n/\partial s \neq 0$) and effect (a flux of particles or individuals, $J \neq 0$). This is indeed intuitively reasonable, because it predicts a vanishing effect ($J = 0$) if the corresponding cause disappears ($\partial n/\partial s = 0$). However, there are more reasonable equations that also have this property. In fact, there should be a time interval between cause and effect. From this perspective, one may expect equation (1) to be replaced by

$$J(x, t+\tau) = -D\frac{\partial}{\partial s}n(x, t), \tag{4}$$

where τ corresponds to the time delay between cause and effect. The well-known fact that linear flux–force dependences (such as Fick's law) are a special, limiting case of time-delayed equations [5] was first noticed by Maxwell [6].

To take another example, the 3D Fourier heat conduction equation

$$\vec{q}(\vec{x}, t) = -\lambda \vec{\nabla} T(\vec{x}, t) \tag{5}$$

predicts that a temperature gradient $\vec{\nabla} T$ causes the instantaneous appearance of a heat flux $\vec{q}$ (λ is the thermal conductivity, $\vec{x}$ is the position vector and t is the time). This physically unpleasant property (instantaneous relation between cause and effect) has been stressed repeatedly. Half a century ago, authors such as Cattaneo [7] and Vernotte [8] proposed to avoid it by letting the heat flux to be time-delayed with respect to the temperature gradient, i.e. a relationship of the form

$$\vec{q}(\vec{x}, t + \tau) = -\lambda \vec{\nabla} T(\vec{x}, t), \tag{6}$$

where τ plays the role of a delay or relaxation time. This equation is the 3D conductive analogue to the 1D diffusive equation (4).

In 3D diffusion phenomena, $\vec{q}$ in equation (6) (or J in equation (4)) is replaced by the diffusion flux $\vec{J}$, T by the particle concentration n, and λ by the diffusion coefficient D,

$$\vec{J}(\vec{x}, t + \tau) = -D \vec{\nabla} n(\vec{x}, t). \tag{7}$$

Time-delayed diffusion has been applied to turbulence [9], propagation of light in turbid media [10], diffusion in glassy polymers [11], photon emission from stellar atmospheres [12], Taylor dispersion [13], radiative transfer [14], etc.

In systems where there is a reactive in addition to a diffusive process, Fickian diffusion leads to parabolic reaction–diffusion (PRD) equations. Equation (3) is the simplest example. Such equations will be derived in section 2 as a special case. However, as first noted by Kac [15], PRD equations are a special case of reaction–diffusion equations, which are based on the instantaneous diffusive effects mentioned above. This unphysical feature can be avoided by making use of hyperbolic reaction–diffusion (HRD) equations. HRD equations have been very recently applied to forest fire models [16], chemical systems [17, 18], crystal growth and solidification fronts [19, 20], thermal combustion [21], human population invasions [22–24] and the spread of virus infections [25]. The most important theoretical prediction is the speed of the wavefronts, which may be compared to the speed measured experimentally.

With some variations [26], hyperbolic equations have been considered to derive the speed of fronts. There are many interesting related problems, such as Turing instabilities [27], spiral waves, patterns, etc. Our review below is focused on the theoretical foundations and methods of solution of the wavefront speed problem, as well as on the specific phenomena mentioned in the previous paragraph—insofar as they pose experimental situations where this problem arises. In all instances where direct comparison between quantitative predictions and experimental values has been performed, it will reported in detail.

Section 2 contains some derivations of the HRD and other fundamental equations. In section 3, we present the most successful theoretical methods which have been applied to the front speed problem for HRD equations. Some applications are reviewed in section 4. The usefulness of the work done in recent years in analysed in sections 6–8. These sections are devoted to the comparison between theoretical predictions and experimental data for several systems of biophysical interest. Finally, section 9 contains a critical discussion and an outline of likely areas of future progress in the field.

2. Microscopic and phenomenological derivations

2.1. Isotropic random walks with reaction

Isotropic random walks in 1D are probably the simplest microscopic model which has been used to derive diffusion equations [28]. Here, we shall extend this approach by including higher-order terms, which will lead us to a hyperbolic equation, and we will also allow for a reactive process.

Let us assume that at time $t = 0$ many particles (animals, viruses, bacteria, etc) are at $x = 0$. Let $n(x, t)$ stand for the density of particles that at time t are at position x. Alternatively, $n(x, t)$ can be defined as the fraction of particles at (x, t). In isotropic random walks, one assumes the same probability for any particle to jump to the left or to the right. Also, in this very simple model one assumes that all jumps have the same length δ and that the particles spend the same time interval T to perform any of the jumps. Then,

$$n(x, t + T) = \tfrac{1}{2}n(x - \delta, t) + \tfrac{1}{2}n(x + \delta, t) + [n(x, t + T) - n(x, t)]_{\text{growth}}, \quad (8)$$

where the last term stands for a reactive contribution, which may correspond, for example, to the reproduction of a living species. In biophysical applications, it is usually referred to as a growth term. Defining $F(n) \equiv [\partial n/\partial t]_{\text{growth}}$ and assuming that the spatial and temporal lengths of jumps are much smaller than the typical dimensions and durations measured experimentally ($T \ll t$, $\delta \ll x$), we may expand the previous equations up to second order to obtain

$$\tau\frac{\partial^2 n}{\partial t^2} + \frac{\partial n}{\partial t} = D\frac{\partial^2 n}{\partial x^2} + F(n) + \tau\frac{\partial F(n)}{\partial t}, \quad (9)$$

which is a HRD equation, central to the present review, with diffusion coefficient

$$D \equiv v^2\tau, \quad (10)$$

where $v \equiv \delta/T$ is the speed of particles, and

$$\tau \equiv \frac{T}{2} \quad (11)$$

is called the relaxation or delay time. We see that, in this model, τ is half the time duration of jumps. Alternatively, in some applications one assumes that T is a resting time between successive jumps, the duration of which is negligible as compared to the time spent by particles when performing a jump (in such an instance, v is of course not the speed of particles when they jump, but it can still be interpreted as a mean speed).

A more restricted approach retains only terms up to first order. Then,

$$\frac{\partial n}{\partial t} = D\frac{\partial^2 n}{\partial x^2} + F(n), \quad (12)$$

which is a PRD equation (see equation (3)). It was originally analysed by Fisher in 1937 [1], and also in 1937 by Kolmogorov *et al* [29].

Another special case is recovered if, again, one keeps only terms up to first order, and also neglects the reactive process. Then,

$$\frac{\partial n}{\partial t} = D\frac{\partial^2 n}{\partial x^2}, \quad (13)$$

which is the well-known evolution equation for Fickian (or non-delayed) diffusion.

More general microscopic models are usually needed to compare theory to observations. Depending on the microscopic movement of particles in a specific experimental situation, the approximation of isotropic jumps may break down (section 2.2). Sometimes, one needs to relax the assumption that the jump or resting time T is the same for all jumps (section 2.6). In other

experiments, assuming that all jumps have the same length δ is not realistic and the particle movement takes place in 2D (section 6.1), etc. However, the very simple model presented above is a very valuable guide to more complicated situations.

2.2. Anisotropic random walks with reaction

When memory effects are taken into account, successive movements of the dispersive particles are not mutually independent, so that there is a correlation between successive steps. This model was developed initially by Goldstein [30] in 1951 starting from a pioneering work by Taylor in 1921 [9]. Following this approach, we now show how to construct a difference equation and its limiting partial hyperbolic differential equation, while allowing for a reactive process [31–33].

Let $n(x,t)$ stand for the fraction of particles that at time t are at position x. Denoting by $n_+(x,t)$ and $n_-(x,t)$ the fraction of particles which are *arriving from* the left and from the right respectively, then

$$n(x,t) = n_+(x,t) + n_-(x,t). \tag{14}$$

We denote by p the probability of jumping in the same direction as the previous jump, i.e. the probability that the particle persists in its direction after completing a step, whereas $q = 1-p$ is the probability for jumping in the opposite direction. Note that in isotropic random walks (section 2.1), the probability of jumping to the right or to the left is $1/2$, so there is no correlation between the speed direction at successive jumps. When movement is correlated p and q depend explicitly on the time of jump T. For small T, one can expand in Taylor series obtaining $p = 1-\lambda T + \mathrm{O}(T^2)$ and $q = \lambda T + \mathrm{O}(T^2)$ where λ is the rate of reversal of direction. Let δ stand for the length of jumps occurring in time intervals of length T. Define now $\gamma \equiv p-q$, the correlation coefficient between two successive steps. Particle reproduction may be introduced in this model by defining ϕ as the fraction of newborn particles. Assuming that the particle reproduction does not depend on the movement direction, ϕ is function of $n_+ + n_-$. Furthermore, we assume that newborn particles have the same probability to perform the first jump to the left or to the right. Therefore,

$$\begin{aligned} n_+(x,t+T) &= pn_+(x-\delta,t) + qn_-(x-\delta,t) + \tfrac{1}{2}\phi(n_+ + n_-), \\ n_-(x,t+T) &= pn_-(x+\delta,t) + qn_+(x+\delta,t) + \tfrac{1}{2}\phi(n_+ + n_-). \end{aligned} \tag{15}$$

In the limit $T \to 0$, $\delta \to 0$, keeping the ratio $\delta/T \to v$ finite (the speed of particles), the correlation coefficient $\gamma \to 1$, and the probability of persistence p tends to unity, whereas the probability q of reversal should tend to zero but one can expand in Taylor series

$$\begin{aligned} (n_+, n_-)(x, t+T) &\simeq (n_+, n_-)(x,t) + T\partial_t\,(n_+, n_-) + \cdots, \\ (n_+, n_-)(x \pm \delta, t) &\simeq (n_+, n_-)(x,t) \pm \delta\partial_x(n_+, n_-) + \cdots. \end{aligned} \tag{16}$$

By using equations (16), we may rewrite (15) in the form

$$\partial_t n_+ + v\partial_x n_+ = \lambda(n_- - n_+) + \frac{1}{2T}\phi(n_+ + n_-), \tag{17}$$

$$\partial_t n_- - v\partial_x n_+ = \lambda(n_+ - n_-) + \frac{1}{2T}\phi(n_+ + n_-). \tag{18}$$

By adding equations (17) and (18), one obtains the particle conservation equation (2)

$$\frac{\partial n}{\partial t} + \frac{\partial J}{\partial x} = F(n), \tag{19}$$

where we have taken into account equation (14) and defined $F \equiv \phi/T$. By subtracting equations (17) and (18), one finds for the particle flux, $J(x,t) = v(n_+ - n_-)$, the following equation:

$$\tau \frac{\partial J}{\partial t} + J = -D\frac{\partial n}{\partial x}, \tag{20}$$

which is a Maxwell–Cattaneo equation with relaxation time

$$\tau \equiv \frac{1}{2\lambda} \tag{21}$$

and diffusion coefficient

$$D \equiv v^2\tau. \tag{22}$$

Combining equations (19) and (20), we find the nonlinear reaction–diffusion equation

$$\tau \frac{\partial^2 n}{\partial t^2} + \frac{\partial n}{\partial t} = D\frac{\partial^2 n}{\partial x^2} + F(n) + \tau \frac{\partial F(n)}{\partial t}, \tag{23}$$

which is the same HRD equation as that for the isotropic random walk (equation (9)). It is very important to note, however, that the microscopic expression for the relaxation time (21) is different from that for the isotropic case (equation (11)). Such microscopic expressions are absolutely necessary in order to compare to experiments (sections 6–8 in the present review).

2.3. Phenomenological derivation

In this section, we illustrate a simple way to derive the HRD equation by assuming a diffusion flux which is time-delayed with respect to the establishment of a diffusive gradient [31]. The balance equation for the density (or, alternatively, the fraction) of particles n in a 1D problem is

$$\frac{\partial n}{\partial t} = -\frac{\partial J}{\partial x} + F(n), \tag{24}$$

where $F(n)$ is the particle-generating source function. The particle flux $J(x,t)$ must take into account the relaxational effect due to the delay of the particles in adopting one definite mean speed and direction to propagate. For instance, memory in the correlation between steps (section 2.2) may be understood macroscopically as a delay in the flux of particles for a given concentration gradient. By extending Fick's law with allowance for a time delay τ (see equation (7)),

$$J(x, t+\tau) = -D\frac{\partial n(x,t)}{\partial x}, \tag{25}$$

and expanding J up to the first order in τ one has

$$\tau \frac{\partial J(x,t)}{\partial t} + J(x,t) = -D\frac{\partial n(x,t)}{\partial x} \tag{26}$$

which is the Maxwell–Cattaneo equation (20). For $\tau \to 0$, we have the special case of Fick's law,

$$J(x,t) = -D\frac{\partial n(x,t)}{\partial x} \tag{27}$$

Combining equations (24) and (25), we find the evolution equation

$$\frac{\partial n(x, t+\tau)}{\partial t} = D\frac{\partial^2 n(x,t)}{\partial x^2} + F[n(x, t+\tau)], \tag{28}$$

and expanding in Taylor series the functions $n(x, t+\tau)$ and $F(x, t+\tau)$ up to first order in τ, we recover the HRD equation (23). Therefore, the macroscopic approach in this section is consistent with the microscopic ones in sections 2.1 and 2.2.

2.4. Thermodynamical derivation

In extended irreversible thermodynamics, one assumes that the entropy density s depends on the classical variables and also the dissipative fluxes [5], in our case $s = s(n, J)$, with n the number density of particles and J the particle flux. In differential form,

$$\mathrm{d}s = \left(\frac{\partial s}{\partial n}\right)\mathrm{d}n + \left(\frac{\partial s}{\partial J}\right)\mathrm{d}J, \tag{29}$$

where

$$\left(\frac{\partial s}{\partial n}\right)_J = -T^{-1}\mu, \qquad \left(\frac{\partial s}{\partial J}\right)_n = -\frac{T^{-1}\alpha}{n}J, \tag{30}$$

μ being the chemical potential per particle and α a scalar function not depending on J at this order of approximation. The generalized Gibbs equation up to the second order in J is then given by

$$\mathrm{d}s = \mathrm{d}s_{\mathrm{eq}} - T^{-1}\frac{\alpha}{n}J\,\mathrm{d}J, \tag{31}$$

and integrating, one has for the generalized entropy

$$s = s_{\mathrm{eq}} - \frac{\alpha}{2Tn}J^2. \tag{32}$$

Combining equations (29) and (30) with the particle balance equation (24) and the balance equation for the entropy, $\dot{s} + \nabla \cdot J^s = \sigma_{\mathrm{syst}}$ [5], we find for the entropy production of the system of particles (with $J^s = -\mu J/T$ as usual [5]),

$$\sigma_{\mathrm{syst}} = -\frac{J}{T}\left[\nabla\mu + \frac{\alpha}{n}\frac{\partial J}{\partial t}\right] - \frac{\mu F}{T}. \tag{33}$$

Let us now notice that the physical volume element contains two subsystems. On the one hand, the particles—which are the centre of our attention—and, on the other, the medium generating new particles. What must be positive-definite according to the second law of thermodynamics is the total entropy production, namely $\sigma_{\mathrm{T}} = \sigma_{\mathrm{syst}} + \sigma_{\mathrm{gen}}$, i.e. the sum of the entropy productions of both subsystems (and not each of them separately). Thus we have

$$\sigma_{\mathrm{T}} = -\frac{J}{T}\left[\nabla\mu + \frac{\alpha}{n}\frac{\partial J}{\partial t}\right] - \frac{\mu F}{T} + \sigma_{\mathrm{gen}} \geqslant 0. \tag{34}$$

Expression (34) shows two contributions, one for each irreversible process present. The first term is related to diffusion, and the last two terms correspond to the creation of particles. As usual in irreversible thermodynamics, each physical *process* must have a positive-definite entropy production,

$$\sigma_{\mathrm{dif}} = -\frac{J}{T}\left[\nabla\mu + \frac{\alpha}{n}\frac{\partial J}{\partial t}\right] \geqslant 0, \tag{35}$$

$$\sigma_{\mathrm{gen}} - \frac{\mu F(n)}{T} \geqslant 0. \tag{36}$$

The inequality in equation (35) constrains the term inside brackets that must depend on the flux J in order for (35) to be positive-definite. In the simplest case, this relation is linear

$$-\left[\nabla\mu + \frac{\alpha}{n}\frac{\partial J}{\partial t}\right] = LJ, \tag{37}$$

with L a positive scalar quantity.

Defining the positive parameters $\tau \equiv \alpha/nL$ and $D \equiv (\partial\mu/\partial n)/L$ as the relaxation time and the diffusion coefficient, respectively, we find for a 1D environment at rest equation (26), which together with equation (24) yields again the HRD equation (23).

It should be noted that the thermodynamical and phenomenological approaches do not yield a prediction for the diffusion parameters τ and D in terms of directly measurable quantities. Indeed, in the derivation above α and μ have not been related to parameters describing the microscopic movement of particles. However, thermodynamics is a very powerful and simple way to derive the possible forms of the transport equations [5] that can be applied to any system, whatever the microscopic mechanisms at work.

2.5. Kinetic derivation

In this section we derive the 1D reaction–telegraph equation for the particle movement from a kinetic point of view [34], by following the ideas due to Othmer *et al* [35–37]. Although most natural species do not live in 1D environments, the reaction diffusion equation we will derive is the governing equation for dispersal in the limit of 2D interfaces with small curvature, and may therefore be viewed as a canonical equation for particle movement. Let $\mathfrak{f}(x, v, t)$ stand for the nonequilibrium distribution function of particles at position x moving with velocity v at time t. As usual in kinetic theory, the number density of particles at x at time t is

$$n(x,t) = \int \mathfrak{f}(x,v,t)\,\mathrm{d}v, \tag{38}$$

and the particle flux is

$$J(x,t) = \int v\mathfrak{f}(x,v,t)\,\mathrm{d}v. \tag{39}$$

Let the contribution to the rate of change of $\mathfrak{f}$ due to reaction or reproduction be given by $F(n)\varphi(v)$, so that new particles with a normalized velocity distribution $\varphi(v)$ appear at a rate depending only on n. Assuming that the velocity changes can be described by a Poisson process of intensity λ, i.e. that the rate at which particles leave a phase space volume centred at (x, v) is $\lambda\mathfrak{f}(x, v, t)$, we have for the net rate at which particles enter the phase space

$$-\lambda\mathfrak{f} + \lambda\int \mathfrak{f}(x,v',t)K(v'\to v)\,\mathrm{d}v',$$

where the kernel $K(v' \to v)$ is the normalized probability of a change of velocity from v' to v. Thus the corresponding Boltzmann equation for the distribution function is

$$\frac{\partial\mathfrak{f}}{\partial t} + v\frac{\partial\mathfrak{f}}{\partial x} = Q(\mathfrak{f}), \tag{40}$$

where $Q(\mathfrak{f})$ describes the interaction processes and plays the role of the reactive and elastic collision terms in kinetic theory,

$$Q(\mathfrak{f}) = F(n)\varphi(v) - \lambda\mathfrak{f} + \lambda\int K(v'\to v)\mathfrak{f}(x,v',t)\,\mathrm{d}v'. \tag{41}$$

In order to derive the macroscopic transport equation corresponding to the particle movement, we proceed in the usual way in kinetic theory. Integrating equation (40) and making use of equation (41), we obtain

$$\frac{\partial n}{\partial t} + \frac{\partial J}{\partial x} = F(n), \tag{42}$$

which is the balance equation for the number density of particles (see equation (2)). We assume for simplicity that the speed v_0 of particles is constant and that only direction reversals are

allowed. So, the diffusion kernel reads $K(v' \to v) = \delta(v + v')$. Multiplying equation (40) by v and integrating, we find that

$$\frac{\partial J}{\partial t} + 2\lambda J = F(n)\langle v\rangle - \frac{\partial}{\partial x}\int v^2 \mathfrak{f}(x, v, t)\,\mathrm{d}v. \tag{43}$$

Assuming the velocities of newborn particles to be $\pm v_0$, with the same probability $1/2$,

$$\varphi(v) = \tfrac{1}{2}\delta(v + v_0) + \tfrac{1}{2}\delta(v - v_0), \tag{44}$$

thus the mean value is $\langle v\rangle = 0$. Defining

$$\mathfrak{f}^+ = \mathfrak{f}(x, +v_0, t), \qquad \mathfrak{f}^- = \mathfrak{f}(x, -v_0, t), \tag{45}$$

we can rewrite equation (38) as $n(x, t) = \mathfrak{f}^+ + \mathfrak{f}^-$ and equation (39) as $J(x, t) = v_0(\mathfrak{f}^+ - \mathfrak{f}^-)$. Therefore, $\mathfrak{f}^+$ and $\mathfrak{f}^-$ may be related to n and J,

$$\mathfrak{f}^+ = \frac{1}{2}\left(n + \frac{J}{v_0}\right), \qquad \mathfrak{f}^- = \frac{1}{2}\left(n - \frac{J}{v_0}\right). \tag{46}$$

On the other hand, the equation for the particle flux, (43), may be written as

$$\frac{\partial J}{\partial t} + 2\lambda J = -v_0^2\frac{\partial n}{\partial x}, \tag{47}$$

where we have applied that $\int \mathrm{d}v\, v^2\mathfrak{f}(x, v, t) = v_0^2(\mathfrak{f}^+ + \mathfrak{f}^-) = v_0^2 n$. Equation (47) has the form of a Maxwell–Cattaneo equation (20) for diffusion processes, namely $\tau\,\partial J/\partial t + J = -D\partial n/\partial x$, with a flux relaxation time given by

$$\tau \equiv \frac{1}{2\lambda} = \frac{T}{2}, \tag{48}$$

with $T = 1/\lambda$ the time interval between successive jumps, and diffusion coefficient

$$D \equiv v_0^2\tau. \tag{49}$$

By combining equations (42) and (47), we obtain the HRD equation

$$\tau\frac{\partial^2 n}{\partial t^2} + [1 - \tau F'(n)]\frac{\partial n}{\partial t} = D\frac{\partial^2 n}{\partial x^2} + F(n). \tag{50}$$

Note that, in contrast to the derivations presented in the previous subsections, here we have not assumed that temporal and spatial variations can be substituted by their corresponding Taylor expansions. Thus, for Poisson processes, the HRD equation is not an approximate but an exact description of the evolution of the system under consideration.

2.6. Derivation from a waiting time distribution

Let $P(x, t)$ be the probability density that particles arrive to the point x at tine t and $\rho(x, t)$ the probability density to find a particle in x at time t. We introduce $\Phi(t')$ as the probability that a particle waits, at least, a time t' before starting a new jump. Then [35]

$$P(x, t) = \int \mathrm{d}x \int_0^t \mathrm{d}t'\psi(x - x', t - t')P(x', t') + \delta(x)\delta(t) + F(x, t), \tag{51}$$

where ψ is the distribution function of jump lengths and waiting times, the term $\delta(x)\delta(t)$ comes from assuming that all particles are at $x = 0$ for $t = 0$, i.e. $P(x, t = 0) = \delta(x)$ [35], $F(x, t)$ plays the role of source term of probabilities and

$$\phi(t) = \int \mathrm{d}x \int_t^\infty \mathrm{d}t'\psi(x, t') = \int_t^\infty \mathrm{d}t'\psi(t'). \tag{52}$$

On the other hand, we may write

$$\rho(x,t) = \int_0^t \mathrm{d}t' P(x',t')\phi(t-t'). \tag{53}$$

Transforming (51) by Fourier–Laplace

$$P(k,s) = \frac{1+F(k,s)}{1-\psi(k,s)}, \tag{54}$$

and transforming equation (53) one gets

$$\rho(k,s) = \Phi(s)\frac{1+F(k,s)}{1-\psi(k,s)}, \tag{55}$$

where $\Phi(s)$ is the Laplace transform of $\Phi(t)$ and is given by

$$\Phi(s) = \frac{1-\varphi(s)}{s}, \tag{56}$$

with $\varphi(s) \equiv \psi(0,s)$. So, from (55) one finds

$$[1-\psi(k,s)]\rho(k,s) = \Phi(s)[1+F(k,s)]. \tag{57}$$

In order to find the evolution equation for the probability $\rho(x,t)$, one must choose the waiting time and jumps length distributions. If one assumes a Gaussian distribution for the length of jumps (either in Fourier or in real space) and an exponential distribution for the waiting times in Laplace space (i.e., a Dirac delta in real time),

$$\psi(k,s) = \mathrm{e}^{-sT}\mathrm{e}^{-\sigma^2 k^2}, \tag{58}$$

where T is the characteristic waiting time before starting a new jump and $\sigma^2 = DT$, with D the diffusion coefficient. For small lengths and waiting times, one can expand in Taylor series to get $\mathrm{e}^{-DTk^2} \simeq 1 - DTk^2$ and $\mathrm{e}^{sT} \simeq 1 + sT + (sT)^2/2$, respectively, and equation (57) adopts the form

$$\tfrac{1}{2}Ts(s\rho(k,s)-1) + s\rho(k,s) - 1 = -Dk^2\rho(k,s) + F(k,s) + \tfrac{1}{2}TsF(k,s), \tag{59}$$

and antitransforming we get

$$\frac{T}{2}\frac{\partial^2\rho}{\partial t^2} + \frac{\partial\rho}{\partial t} = D\frac{\partial^2\rho}{\partial x^2} + F + \frac{T}{2}\frac{\partial F}{\partial t}, \tag{60}$$

which is again the HRD equation (9), with $\tau = T/2$.

We stress that different derivations are needed in order to be able to obtain specific values for the parameters τ and D, depending on the experiment at hand. For a given experimental result that one seeks to explain, the derivation chosen should be that which best describes the microscopic motion of the particles or living organisms. If the resting time is not approximately the same for all jumps, then a derivation of the HRD equation in the lines explained in this subsection is certainly necessary before one can attempt to compare the theoretical predictions (section 3) to experimental data.

2.7. Additional derivations

Other derivations of the HRD equation have been proposed. A particularly appealing one is based on Einstein's theory of Brownian motion. When properly generalized, Einstein's approach allows to relate the delay time τ to data that can be determined directly from experiments in spaces of more than one dimension, and with jumps of unequal length. That derivation will be presented in section 5.1 in its proper context. Another derivation is based on considering a Poisson branching processes [36].

3. Methods of solution to the front speed problem

For an arbitrary number of spatial dimensions, the conservation equation of the particle number, equation (2), reads

$$\frac{\partial n}{\partial t} + \vec{\nabla} \cdot \vec{J} = F(n), \tag{61}$$

where $n(\vec{x}, t)$ is the number density of particles. Equation (61) holds independently of whether diffusion is Fickian (equation (27)), hyperbolic (equation (27)), etc. Indeed, integration of equation (61) over the volume V of the system yields

$$\frac{\mathrm{d}N}{\mathrm{d}t} = \int_V F(n)\,\mathrm{d}V - \oint_S \vec{J} \cdot \mathrm{d}\vec{s}, \tag{62}$$

which simply states that the change in the total number of particles $N(t) = \int_V n(\vec{x}, t)\,\mathrm{d}V$ is due to the reactive process (first term in the right-hand side) and/or to the particles crossing the boundary surface S of the system (last term). For an isolated system, this boundary term vanishes and

$$\frac{\mathrm{d}N}{\mathrm{d}t} = \int_V F(n)\,\mathrm{d}V. \tag{63}$$

Equilibrium states ($\mathrm{d}N/\mathrm{d}t = 0$) then satisfy the condition

$$F(n) = 0. \tag{64}$$

For illustration purposes, consider the logistic source function

$$F(n) = An - Bn^2, \tag{65}$$

which compares favourably to experimental data for many biological species [38]. The parameter $A = \mathrm{d}F/\mathrm{d}n|_{n=0}$ is called the initial growth rate. The equilibrium states of (65) are $n = 0$ and $n = A/B$.

In order to introduce the concept of stability, consider first the simple case of an homogeneous system (n depends on t but not on $\vec{x}$). The evolution equation for the total number of particles (63) may be written as

$$\frac{\mathrm{d}N}{\mathrm{d}t} = AN\left(1 - \frac{b}{A}N\right), \tag{66}$$

with $b \equiv B/V$. The solution to this equation under the initial condition $N(t = 0) = N_0$ is

$$N(t) = N_0 \frac{N_\infty \mathrm{e}^{At}}{N_\infty + N_0(\mathrm{e}^{At} - 1)}, \tag{67}$$

where $N_\infty = A/b$ is called the carrying capacity, and is the value to which the population number N tends as $t \to \infty$. Therefore, any initial condition $N(t = 0) = N_0$ will evolve towards the equilibrium state $N = N_\infty$ (or $n = A/B$), which is called stable. On the other hand, any initial condition close to the other equilibrium state of (66), namely $N = 0$, will evolve away from it. Therefore, the equilibrium state $N = 0$ (or $n = 0$) is called unstable.

Now consider an inhomogeneous system. A wavefront can be defined as a solution $n(x, t)$ of constant shape and speed connecting two equilibrium states (see figure 1). Usually it is not possible to determine the front shape analytically, but in many applications the available experimental data refer to its propagation speed v (see figure 1). In this section, we will discuss the most useful methods that can be used to predict the front speed for HRD equations.

If the delay time is neglected ($\tau \simeq 0$ in equation (9)), the evolution equation is

$$n_t = n_{xx} + f(n), \tag{68}$$

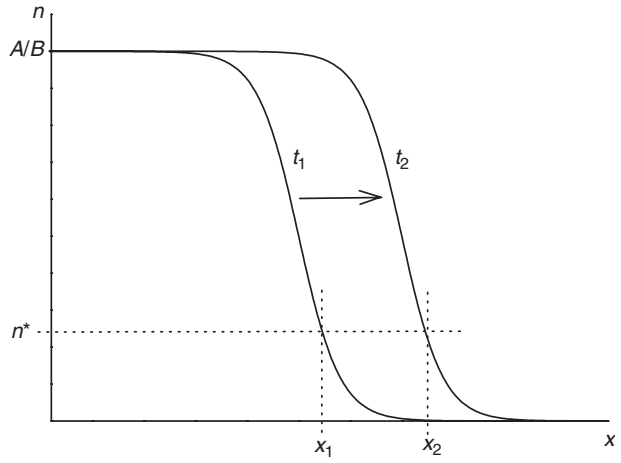

Figure 1. Wavefront connecting two equilibrium states and moving to the right. Wavefronts correspond to the local evolution of the population density from an unstable state to an stable one. For a logistic growth function (equation (65)), these states are $n = 0$ (unstable) and $n = A/B$ (stable or final state). Since the asymptotic ($t \to \infty$) shape of fronts is constant, in this figure n^* can have any value such that $0 < n^* < A/B$. The speed of the front is $v = (x_2 - x_1)/(t_2 - t_1)$.

where n is the density of particles or living organisms. Equations of this kind are called PRD equations. It has been shown by Aronson and Weinberger [39] that sufficiently localized initial conditions evolve asymptotically into a travelling monotonic wavefront. It is observed both experimentally and numerically that the global, nonlinear dynamics rapidly selects a unique solution. The speed c at which the front moves towards the stable state is referred to as the selected speed.

For PRD equations, there already exist several proposed criteria in the literature for the analysis of the dynamical velocity selection: a minimum speed rule [40], structural stability [41], marginal stability [40, 42], and many others. Below we shall present several methods to study the speed of HRD equations. The results for PRD equations ($\tau \to 0$) will be recovered as special cases.

It is convenient to rescale equation (9) for further purposes as follows:

$$t^* = kt, \tag{69}$$

$$x^* = x\sqrt{\frac{k}{D}}, \tag{70}$$

and write

$$F(n) \equiv kf(n), \tag{71}$$

where $1/k$ is a characteristic time of the reactive process. We define

$$a \equiv k\tau. \tag{72}$$

Then equation (9) becomes, omitting asterisks for notational simplicity,

$$a\partial_{tt}n + \partial_t n = \partial_{xx}n + f(n) + af'(n)\partial_t n. \tag{73}$$

In the following subsections we illustrate different methods to find bounds or, in some cases, the exact asymptotic speed,

$$v = c\sqrt{kD} \tag{74}$$

for wavefront solutions to HRD equations.

3.1. Linear analysis

Assume that equation (73) has travelling wavefronts with profile $n(x - ct)$ and moving with a dimensionless speed $c > 0$. It will satisfy the equation

$$(1 - ac^2)n_{zz} + c[1 - af'(n)]n_z + f(n) = 0, \tag{75}$$

where $z = x - ct$, and with boundary conditions $\lim_{z\to\infty} n = 0$, $\lim_{z\to-\infty} n = 1$, and $n_z < 0$ in (0, 1); we also assume that n_z vanishes for $z \to \pm\infty$ [33]. We will now analyse how linear stability analysis can be applied to HRD equations, in order to study the speed of the front.

Linear analysis makes it possible to study the behaviour of the wavefront near the equilibrium states (n = constant), which according to equation (9) are the solutions to the equation $f(n) = 0$, say $n = 0$ and $n = 1$ (e.g. for the logistic growth, one may define $n^* \equiv Bn/A$ so the equilibrium states are $n^* = 0$ and $n^* = 1$). In [31] the lower bound for c was derived by analysing the trajectories in the phase space (n, n_z) [28]. Here we will summarize an alternative approach that yields the same conditions on the front velocity but, in contrast to the one in [31], it will allow us to analyse the asymptotic behaviour of $n(z)$ near the equilibrium points [43]. This behaviour will in turn be used in the derivation of better bounds on the speed in section 3.3.

3.1.1. $n \approx 0$. Setting $\epsilon(z) = n(z) \ll 1$, we linearize equation (75) to obtain the front equation near $n = 0$. We get

$$(1 - ac^2)\epsilon_{zz} + c[1 - af'(0)]\epsilon_z + f'(0)\epsilon = 0. \tag{76}$$

Solutions of the form $\epsilon \sim e^{\lambda z}$ provide us with the following characteristic equation:

$$(1 - ac^2)\lambda^2 + c[1 - af'(0)]\lambda + f'(0) = 0. \tag{77}$$

So, the solution of the linearized equation (76) near $n = 0$ is given by

$$\epsilon(z) = A_+ e^{\lambda_+ z} + A_- e^{\lambda_- z} \tag{78}$$

where A_+ and A_- are integration constants (depending on the initial and boundary conditions) and $\lambda_\pm$ are the solutions of the characteristic equation (77). Since $\epsilon(z) = n(z)$ is the number density of particles, it cannot be negative for any possible value of z, thus $\lambda_\pm \in \mathbb{R}$. It therefore follows from equation (77) that c has a lower bound c_L given by

$$c \geqslant c_L = \frac{2\sqrt{f'(0)}}{1 + af'(0)}, \tag{79}$$

where it has been assumed that $f'(0) > 0$. If this does not hold, the approach we shall present in this section breaks down. This happens, for example, in forest fire models (section 4.4), and in such cases one may resort the variational analysis we will develop in section 3.3.

For the parabolic case ($\tau \to 0$), equation (79) becomes

$$c_{\tau\to 0} \geqslant 2\sqrt{f'(0)}, \tag{80}$$

which is the classical result due to Fisher [1]. In the analysis of combustion waves [44], it is often referred to as the Kolmogorov–Petrovski–Piskunov (KPP) value [29].

In the limit $z \to +\infty$ one has $n \to 0$ as boundary condition, so $\lambda_\pm$ must be negative. If one (or both) values of λ were positive, then in the limit $z \to +\infty$ one would have $n \to +\infty$ and we would not be dealing with a solution connecting the equilibrium states $n = 1$ and $n = 0$, thus the solution under consideration would not satisfy the definition of wavefront, given at the beginning of section 3. Therefore equation (77) yields the conditions

$$c < \frac{1}{\sqrt{a}}, \tag{81}$$

$$1 - af'(0) > 0. \tag{82}$$

3.1.2. $n \approx 1$. We now introduce $\epsilon(z) = 1-n(z) > 0$ and $f(n) \simeq -f'(1)(1-n) = |f'(1)|\epsilon$, assuming $f'(1) < 0$ (in biological applications $f(n)$ is always to observed to satisfy this condition [38]). The linearized equation (75) near $n = 1$ is

$$(1 - ac^2)\epsilon_{zz} + c[1 + a|f'(1)|]\epsilon_z - |f'(1)|\epsilon = 0. \tag{83}$$

This equation holds for $n \approx 1$ and is the analogue to equation (76), which holds for $n \approx 0$. Similarly, for $n \approx 1$ equations (77) and (78) are replaced by

$$(1 - ac^2)\lambda^2 + c[1 + a|f'(1)|]\lambda - |f'(1)| = 0, \tag{84}$$

$$\epsilon(z) = B_+ e^{\lambda_+ z} + B_- e^{\lambda_- z}, \tag{85}$$

respectively. Here we note that there are real two solutions for λ, one of them being positive (say λ_+) and the other one negative (say λ_-). Thus, contrary to what happened in the case $n \approx 0$ (where λ_+ and λ_- could both be required to be negative in order to ensure that $n \to 0$ for $z \to \infty$ for arbitrary initial conditions), here we have $\lambda_+ > 0$ and $\lambda_- < 0$. Now since we must require that $n \to 1$ for $z \to -\infty$, we see that it is necessary that $B_- = 0$, i.e. for $n \approx 1$ only $\lambda_+ > 0$ will appear in the asymptotic solution (85), whereas for $n \approx 0$ both $\lambda_+ < 0$ and $\lambda_- < 0$ appear in the corresponding solution (78). This general result is in agreement with an explicit solution, which was derived previously for a very specific source term $f(n)$ and initial condition (see section V in [31]).

Just to summarize, the linear analysis presented in this section shows the existence of a travelling wavefront, connecting the equilibrium states $n = 0$ and $n = 1$, provided that $f'(0) > 0$ and that the front satisfies the conditions (79), (81) and (82).

3.2. Marginal-stability analysis

The marginal-stability approach (MSA) was studied initially by Dee and Langer [40] and Ben-Jacob *et al* [42]. In this subsection, we shall show how the MSA performed by van Saarloos for PRD equations [45] may be extended to HRD equations.

The velocity c^* corresponding to MSA can be determined explicitly from a simple analysis in the leading edge of the profile. If $\omega(k)$ is the dispersion relation of the linear portion of the HRD equation (9), where ω and k are complex, the front has an envelope which moves with a velocity $\mathrm{Re}\,\omega(k)/\mathrm{Re}\,k$. For the leading edge, stability with respect to small changes in the wave vector requires $\mathrm{Im}(\mathrm{d}\omega/\mathrm{d}k) = 0$. The profile is marginally stable when the envelope velocity is also equal to $\mathrm{d}\omega/\mathrm{d}k$. Hence if the selected velocity corresponds to the marginal stability velocity c^*, we have

$$c^* = \frac{\mathrm{Re}\,\omega(k^*)}{\mathrm{Re}\,k^*} = \left(\frac{\mathrm{d}\omega}{\mathrm{d}k}\right)_{k=k^*}, \tag{86}$$

$$\mathrm{Im}\left(\frac{\mathrm{d}\omega}{\mathrm{d}k}\right)_{k=k^*} = 0. \tag{87}$$

These equations determine k^* and c^*. The dispersion relation $\omega(k)$ may be obtained by inserting $n \sim \exp[\omega t - kx]$ into the linear part of equation (73) [$f(n) \simeq f'(0)n$]. This yields

$$a\omega^2 + \omega = k^2 + f'(0) + af'(0)\omega. \tag{88}$$

Since ω and k are complex, we define $\omega = \omega_\mathrm{r} + \mathrm{i}\omega_\mathrm{i}$ and $k = k_\mathrm{r} + \mathrm{i}k_\mathrm{i}$, where the subscripts r and i denote the real and imaginary part, respectively. Defining the following quantities

$$\alpha_\mathrm{r} = (1 + af'(0))^2 + 4a(k_\mathrm{r}^2 - k_\mathrm{i}^2),$$
$$\alpha_\mathrm{i} = 8ak_\mathrm{r}k_\mathrm{i},$$

$$\beta_{\rm r} = \frac{1}{\sqrt{2}}\left[\sqrt{\alpha_{\rm r}^2+\alpha_{\rm i}^2}+\alpha_{\rm r}\right]^{1/2},$$
$$\beta_{\rm i} = \frac{1}{\sqrt{2}}\left[\sqrt{\alpha_{\rm r}^2+\alpha_{\rm i}^2}-\alpha_{\rm r}\right]^{1/2}, \tag{89}$$

we obtain the real and imaginary parts of ω:

$$\omega_{\rm r} = \frac{-1+af'(0)\pm\beta_{\rm r}}{2a}, \qquad \omega_{\rm i} = \pm\frac{\beta_{\rm i}}{2a}. \tag{90}$$

So, from equation (87),

$$\mathrm{Im}\left(\frac{{\rm d}\omega}{{\rm d}k}\right) = \frac{2(k_{\rm i}\beta_{\rm r}-k_{\rm r}\beta_{\rm i})}{\beta_{\rm r}^2+\beta_{\rm i}^2} = 0, \tag{91}$$

which is fulfilled if $\beta_{\rm i}=0$ and $k_{\rm i}=0$ (see equation (89)). From the first equation in (89) we obtain an equation for $k_{\rm r}$ which may be solved to yield

$$k_{\rm r}^* = \sqrt{f'(0)}\frac{1+af'(0)}{1-af'(0)}, \tag{92}$$

and from equations (86) and (90)

$$c^* = \frac{\omega_{\rm r}}{k_{\rm r}} = \frac{2\sqrt{f'(0)}}{1+af'(0)}, \tag{93}$$

which provides an assessment of the result obtained by the linear analysis near the equilibrium unstable state (equation (79)). We conclude that, for HRD equations, either of both methods can be used provided that $f(0)=0$ and $f'(0)>0$. However, for some important source functions $f(n)$ one has $f'(0)=0$. Then one must seek alternative approaches, such as the variational one presented in the next subsection.

3.3. Variational analysis

In this section we show how the variational analysis proposed by Benguria and Depassier for PRD equations [46] can be extended to HRD equations [43]. We start from equation (75) and define $p(n)=-n_z$ with $p(0)=p(1)=0$ and $p>0$ in $(0,1)$. Equation (75) may be written as

$$(1-ac^2)p\frac{{\rm d}p}{{\rm d}n} - c[1-af'(n)]p + f(n) = 0. \tag{94}$$

Let $g(n)$ be an arbitrary positive function. Multiplying equation (94) by g/p and integrating by parts we obtain

$$c\int_0^1 g(1-af'(n))\,{\rm d}n = \int_0^1\left[(1-ac^2)hp+\frac{gf}{p}\right]{\rm d}n \tag{95}$$

where $h=-g'>0$, as chosen for PRD equations [47]. Now for any positive numbers r and s, it follows from $(r-s)^2\geqslant 0$ that $(r+s)\geqslant 2\sqrt{rs}$. If $1-ac^2>0$ or $c<1/\sqrt{a}$, since f, g, h, and p are positive, we may choose $r\equiv(1-ac^2)hp$ and $s\equiv gf/p$ to get a restriction on c which eliminates p,

$$(1-ac^2)hp+\frac{gf}{p}\geqslant 2\sqrt{1-ac^2}\sqrt{fgh}, \tag{96}$$

and therefore

$$\frac{c}{\sqrt{1-ac^2}}\geqslant 2\frac{\int_0^1\sqrt{fgh}\,{\rm d}n}{\int_0^1 g(1-af'(n))\,{\rm d}n}. \tag{97}$$

If the effect of the delay time τ is neglected (i.e. for $a = k\tau \approx 0$), this reduces to the Benguria–Depassier principle [46,47]. To see that equation (97) is a variational principle, we must show that there is a function $g = \hat{g}$ for which the equality holds. From the explanation above equation (96) we see that this happens when $r = s$ or

$$(1 - ac^2)\hat{h}p = \frac{\hat{g}f}{p}, \tag{98}$$

which according to our HRD equation (94) implies that $\hat{g}$ satisfies the ordinary differential equation

$$\frac{\hat{g}'}{\hat{g}} = -\frac{c}{1 - ac^2}\frac{1 - af'(n)}{p} + \frac{p'}{p}. \tag{99}$$

The corresponding $\hat{g}$, obtained by integrating this equation, is given by

$$\hat{g}(n) \sim p(n) \exp\left[-\frac{c}{1 - ac^2}\int_{n_0}^{n} \frac{1 - af'(\tilde{n})}{p}\,\mathrm{d}\tilde{n}\right] \tag{100}$$

with $0 < n_0 < 1$. Evidently $\hat{g}(n)$ is a continuous positive function. We will now determine the behaviour of $\hat{g}(n)$ near $n = 0$ and see that the integrals in equation (97) exist. To verify this we recall, from the linear analysis, that the front approaches $n = 0$ exponentially. From this, it is easily seen that the dominant term in equation (78) yields $p = -\mathrm{d}n/\mathrm{d}z \sim \mu n$, where

$$\mu = \frac{1}{2(1 - ac^2)}[c(1 - af'(0)) + \sqrt{c^2(1 + af'(0))^2 - 4f'(0)}]. \tag{101}$$

For $\tau \to 0$ this reduces, as it should, to the result derived for PRD equations by Aronson and Weinberger [39] (see also [47]). Thus, from equation (100) we get, near $n = 0$,

$$\hat{g}(n) \sim n^{1-\gamma}, \tag{102}$$

where

$$\gamma = \frac{c(1 - af'(0))}{\mu(1 - ac^2)}. \tag{103}$$

We also get in this limit $\sqrt{f\hat{g}\hat{h}} \sim \hat{g}f'(n) \sim n^{1-\gamma}$. Hence the integrals in equation (97) exist if $\gamma < 2$. This condition is satisfied provided that

$$c > \frac{2\sqrt{f'(0)}}{1 + af'(0)}, \tag{104}$$

which is in agreement with the lower bound (79) derived form the linearization method. But this is only a lower bound. As we shall see, the lower bound is often different from the true speed (this is also true for PRD equations [44]). Thus, the variational method goes much further than those in sections 3.1 and 3.2. Indeed, the *exact* asymptotic speed of the front may in principle be computed from

$$\frac{c}{\sqrt{1 - ac^2}} = \max_{g}\left(2\frac{\int_0^1 \sqrt{fgh}\,\mathrm{d}n}{\int_0^1 g(1 - af'(n))\,\mathrm{d}n}\right). \tag{105}$$

Below we shall see how this maximization is performed in order to obtain lower and upper bounds and, in some case, the exact value of c.

It is important to notice that the variational result given by equation (105) requires two strong conditions in order to be applicable, namely

$$c < \frac{1}{\sqrt{a}} \tag{106}$$

and

$$1 - af'(n) > 0. \tag{107}$$

The second restriction is equivalent to $a < 1/M$, with $M = \max_{n\in(0,1)} f'(n)$, and will be used explicitly in the derivation of upper bounds for the front velocity (subsection 2 below). In the following two subsections, we analyse whether the variational result leads to lower and upper bounds for the asymptotic speed and compare to the linear (and marginal stability) results from sections 3.1 and 3.2. We shall also show that the variational result (105) makes it possible to obtain a better upper bound on the speed than that following from linear stability or the general variational arguments above, i.e. $c < c_{\max} = 1/\sqrt{a}$ (see equation (81) or (106)).

3.3.1. Lower bounds. In this section we will present a simple example on the variational derivation of lower bounds. We will consider the simple case in which $f'(0) > 0$, and rederive equation (79). Although that result has been already derived above, the method we will present turns out to be a very useful guide to more complicated cases such as upper bounds. It will also be valuable in order to find out lower bounds if $f'(0) = 0$, a relevant case for which the methods in the previous sections break down altogether (this will be discussed in detail in section 4.4).

As we have mentioned in the study above, one may obtain a lower bound for the asymptotic speed by means of a given function $g(n)$. This trial function must satisfy that $g(n) > 0$ and $g'(n) < 0$ in $(0, 1)$. Consider the simple sequence of trial functions $g = n^{\alpha-1}$ in the limit $\alpha \to 0$. These functions are positive and have negative derivative for $0 \leqslant \alpha < 1$, as required in the derivations in section 3.3 above. According to equation (97) or (105),

$$\frac{c}{\sqrt{1-ac^2}} \geqslant 2\sqrt{1-\alpha}\,\frac{\int_0^1 n^{\alpha-3/2}\sqrt{f(n)}\,\mathrm{d}n}{\int_0^1 n^{\alpha-1}[1-af'(n)]\,\mathrm{d}n}. \tag{108}$$

In the limit $\alpha \to 0$, the integrands diverge at $n = 0$, as in the case of PRD equations [46], thus only the singular point will contribute in the limit. The surviving contributions are then

$$\frac{c}{\sqrt{1-ac^2}} \geqslant 2\sqrt{1-\alpha}\,\frac{\int_0^\varepsilon n^{\alpha-3/2}\sqrt{f(n)}\,\mathrm{d}n}{\int_0^\varepsilon n^{\alpha-1}[1-af'(n)]\,\mathrm{d}n}. \tag{109}$$

We may expand the integrands in Taylor series near $n = 0$. Only the leading term in the expansions will contribute as $\alpha \to 0$ and we have, assuming $f'(0) > 0$,

$$\frac{c}{\sqrt{1-ac^2}} \geqslant 2\sqrt{1-\alpha}\,\frac{\int_0^\varepsilon n^{\alpha-3/2}\sqrt{f'(0)n}\,\mathrm{d}n}{\int_0^\varepsilon n^{\alpha-1}[1-af'(0)]\,\mathrm{d}n}. \tag{110}$$

Performing the integrals and taking the limit $\alpha \to 0$ we obtain

$$\frac{c}{\sqrt{1-ac^2}} \geqslant \frac{2\sqrt{f'(0)}}{1-af'(0)}, \tag{111}$$

thus

$$c \geqslant c_{\mathrm{L}} = \frac{2\sqrt{f'(0)}}{1+af'(0)}. \tag{112}$$

This reduces, as it should, to the classical or PRD value $c_{\mathrm{L}} = 2\sqrt{f'(0)}$ [1, 29, 39] if the effect of the delay time is neglected ($a \approx 0$). It is seen that the lower bound (112) is the same as equation (79), which is also known from the derivation of the variational principle above. We conclude that the variational principle we have derived does not provide better lower bounds for the speed of wavefronts than the linear or MSA approaches if we choose

$g(n) = n^{\alpha-1}$. As we shall see in detail in the following subsection, the opposite happens for upper bounds. Moreover, the method presented above for $g(n) = n^{\alpha-1}$ is of interest since it does yield better lower bounds for other trial functions $g(n)$, depending on the source function considered (an explicit example will be presented in section 4.4).

3.3.2. Upper bounds. By extending the PRD development by Benguria and Depassier [46], it is possible to derive upper bounds for the asymptotic speed of HRD equations [43]. We need the particular case of Jensen's inequality [48]

$$\frac{\int_0^1 \mu(n)\sqrt{\alpha(n)}\,\mathrm{d}n}{\int_0^1 \mu(n)\,\mathrm{d}n} \leqslant \sqrt{\frac{\int_0^1 \mu(n)\alpha(n)\,\mathrm{d}n}{\int_0^1 \mu(n)\,\mathrm{d}n}} \tag{113}$$

where $\mu(n) > 0$ and $\alpha(n) \geqslant 0$. If we define

$$\mu(n) \equiv g(n)[1 - af'(n)] \tag{114}$$

and

$$\alpha(n) \equiv \frac{f(n)h(n)}{g(n)(1 - af'(n))^2}, \tag{115}$$

then the left-hand side of the inequality (113) may be written as

$$\frac{\int_0^1 \mu(n)\sqrt{\alpha(n)}\,\mathrm{d}n}{\int_0^1 \mu(n)\,\mathrm{d}n} = \frac{\int_0^1 \sqrt{fgh}\,\mathrm{d}n}{\int_0^1 g(1 - af')\,\mathrm{d}n}, \tag{116}$$

and inside the square root in the right-hand side we have

$$\frac{\int_0^1 \mu(n)\alpha(n)\,\mathrm{d}n}{\int_0^1 \mu(n)\,\mathrm{d}n} = \frac{\int_0^1 [fh/(1 - af')]\,\mathrm{d}n}{\int_0^1 g(1 - af')\,\mathrm{d}n}. \tag{117}$$

Then, from equations (105) and (113), we obtain a relatively simple expression which will allow us to find upper bounds,

$$\frac{c}{\sqrt{1 - ac^2}} = 2\max_g \left(\frac{\int_0^1 \sqrt{fgh}\,\mathrm{d}n}{\int_0^1 g(1 - af')\,\mathrm{d}n} \right) \leqslant 2\max_g \left[\frac{\int_0^1 [fh/(1 - af')]\,\mathrm{d}n}{\int_0^1 g(1 - af')\,\mathrm{d}n} \right]^{1/2}. \tag{118}$$

We now observe that integration by parts makes it possible to find an expression in which $h = g'$ no longer appears,

$$\int_0^1 \frac{fh}{1 - af'}\,\mathrm{d}n = \int_0^1 g\frac{f' + a(ff'' - f'^2)}{(1 - af')^2}\,\mathrm{d}n. \tag{119}$$

Moreover, in order to get an upper bound independent of g, we write equation (119) in a more useful form,

$$\begin{aligned} \int_0^1 \frac{fh}{1 - af'}\,\mathrm{d}n &= \int_0^1 g(1 - af')\frac{f' + a(ff'' - f'^2)}{(1 - af')^3}\,\mathrm{d}n \\ &\leqslant \sup_{n\in(0,1)} \left[\frac{f' + a(ff'' - f'^2)}{(1 - af')^3} \right] \int_0^1 g(1 - af')\,\mathrm{d}n, \end{aligned} \tag{120}$$

were we have applied the condition $(1 - af') > 0$. Finally,

$$\frac{c}{\sqrt{1 - ac^2}} \leqslant 2\sqrt{\sup_{n\in(0,1)} \Psi(n)} \tag{121}$$

where

$$\Psi(n) \equiv \frac{f' + a(ff'' - f'^2)}{(1 - af')^3}. \tag{122}$$

Hence the upper bound may be written as

$$c_{\mathrm{U}} = \frac{2q(a)}{\sqrt{1 + 4aq^2(a)}} \tag{123}$$

where $q(a) = \sqrt{\sup_{n\in(0,1)} \Psi(n)}$. This result may be written in a simpler form if we assume that the source function $f(n)$ is continuous and such that $f'' < 0$ in $(0, 1)$. Then, since $f(0) = f(1) = 0$ we have $f'(0) > 0$ and $f'(1) < 0$. We may write

$$\Psi(n) = \frac{f'}{(1 - af')^2} + a\frac{ff''}{(1 - af')^3} \tag{124}$$

where, recalling the condition $1 - af'(n) > 0$, we see that the second term is negative (it only vanishes at $n = 0, 1$). Moreover, since we have assumed that f is continuous and that $f'' < 0$, the first term decreases for increasing values of n. Thus,

$$\sup_{n\in(0,1)} \Psi(n) = \frac{f'(0)}{(1 - af'(0))^2},$$

and we have the simpler result

$$c \leqslant c_{\mathrm{U}} = \frac{2\sqrt{f'(0)}}{1 + af'(0)}, \tag{125}$$

which holds provided that f is continuous and $f'' < 0$ in $(0, 1)$. Some examples are discussed in section 4. We note that the lower and upper bounds are the same (see equation (112)), so the asymptotic speed may be predicted without uncertainty

$$c = \frac{2\sqrt{f'(0)}}{1 + af'(0)}. \tag{126}$$

This generalizes the corresponding theorem for PRD equations ($a = 0$), which states that the exact wavefront speed is $c_{\tau=0} = 2\sqrt{f'(0)}$ provided that $f(n)$ is continuous and that $f'' < 0$ in $(0, 1)$ [39, 47]. Note that the effect of the delay time is to reduce the wavefront speed, $c < c_{\tau=0}$, as it was to be expected intuitively.

The method presented in this subsection will be applied to the case $f'(0) = 0$ in section 4.4.

3.4. Hamilton–Jacobi dynamics

Fedotov has applied Hamilton–Jacobi dynamics to the front speed problem [49] as follows. In the long-time, large-distance behaviour of the travelling-wave solution to equation (9) from the initial condition $n(0, x) = \theta(x)$, where $\theta(x)$ is the Heaviside function, it is convenient to make the scaling $t \to t/\varepsilon$ and $x \to x/\varepsilon$, where ε is a small parameter. We can write then equation (9) in the form of a Cauchy problem,

$$\begin{aligned} &\tau\varepsilon\partial_{tt}n^\varepsilon + \partial_t n^\varepsilon = \varepsilon D\partial_{xx}n^\varepsilon + \frac{F(n^\varepsilon)}{\varepsilon} + \tau F'(n^\varepsilon)\partial_t n^\varepsilon, \\ &n^\varepsilon(x, 0) = \theta(x), \end{aligned} \tag{127}$$

where $n^\varepsilon(x, t) \equiv n(x/\varepsilon, t/\varepsilon)$. The problem is now to derive the equation governing the position of the front. This can be done by replacing $n^\varepsilon(x, t)$ by an auxiliary field $G^\varepsilon(x, t) \geqslant 0$ through the exponential transformation

$$n^\varepsilon(x, t) \equiv \exp\left[-\frac{G^\varepsilon(x, t)}{\varepsilon}\right].$$

We expect that the profile develops into a wavefront, i.e. that $n^\varepsilon(x,t)$ tends to a unit step function $\theta(x-vt)$ as $\varepsilon \to 0$. The goal is to find a function $G^\varepsilon(x,t)$ determining the position of the front, such that

$$\lim_{\varepsilon\to 0} n^\varepsilon(x,t) = \begin{cases} 0 & G^\varepsilon(x,t) > 0, \\ 1 & G^\varepsilon(x,t) = 0. \end{cases}$$

Straightforward calculations show that $G^\varepsilon(x,t)$ satisfies the equation

$$\tau(\partial_t G^\varepsilon)^2 - \tau\varepsilon\partial_{tt}G^\varepsilon - \left[1 - \tau\frac{\mathrm{d}F(G^\varepsilon)}{\mathrm{d}G^\varepsilon}\right]\partial_t G^\varepsilon = D(\partial_x G^\varepsilon)^2 - \varepsilon D\partial_{xx}G^\varepsilon + F(G^\varepsilon)\exp\left[\frac{G^\varepsilon(x,t)}{\varepsilon}\right]. \tag{128}$$

Taking the limit $\varepsilon \to 0$, we may conclude from equation (128) that the limiting function $G(x,t) = \lim_{\varepsilon\to 0} G^\varepsilon(x,t)$ obeys the first-order, nonlinear partial differential equation

$$\tau(\partial_t G)^2 - \left[1 - \tau\lim_{\varepsilon\to 0}\frac{\mathrm{d}F(G^\varepsilon)}{\mathrm{d}G^\varepsilon}\right]\partial_t G = D(\partial_x G)^2 + \lim_{\varepsilon\to 0} F(G)\exp\left[\frac{G(x,t)}{\varepsilon}\right].$$

We consider source functions of the form $F(n) = knb(n)$ such that

$$\max_{n\in[0,1]} b(n) = b(0) = 1 \qquad \text{and} \qquad b(1) = 0, \tag{129}$$

as for instance the generalized logistic source $F(n) = kn(1-n^p)$. Therefore,

$$\lim_{\varepsilon\to 0}\frac{\mathrm{d}F(G^\varepsilon)}{\mathrm{d}G^\varepsilon} = \lim_{\varepsilon\to 0} F(G)\exp\left[\frac{G(x,t)}{\varepsilon}\right] = k$$

and finally,

$$(\partial_t G)^2 - \frac{\alpha}{\tau}\partial_t G - \frac{D}{\tau}(\partial_x G)^2 - \frac{k}{\tau} = 0. \tag{130}$$

On the other hand, the relativistic Hamilton–Jacobi equation for a particle with mass M moving in the potential field V is [50]

$$(\partial_t G + V)^2 - M^2c^4 - c^2(\partial_x G)^2 = 0. \tag{131}$$

with an associated Hamiltonian

$$H = \sqrt{M^2c^4 + c^2p^2} + V, \tag{132}$$

where $H \equiv -\partial_t G$, $p \equiv \partial_x G$ and c is the speed of light.

By comparing equation (131) with (130) one has

$$V = -\frac{1-\tau k}{2\tau}, \tag{133}$$

$$c = \sqrt{\frac{D}{\tau}}, \tag{134}$$

$$M^2 = \frac{(1-\tau k)^2/4\tau^2 + k/\tau}{c^4}. \tag{135}$$

The solution of (131) is

$$G(x,t) = \min_{x(0)=x, x(t)=0}\left[\int_0^t L(x,s)\,\mathrm{d}s\right], \tag{136}$$

where the Lagrangian L has the form

$$L(x,s) = -Mc^2\sqrt{1 - \frac{1}{c^2}\left(\frac{\mathrm{d}x}{\mathrm{d}s}\right)^2} - V. \tag{137}$$

The optimal trajectory satisfies the Euler–Lagrange equation

$$\frac{\mathrm{d}}{\mathrm{d}s}\left(\frac{\partial L}{\partial \dot{x}}\right) - \frac{\partial L}{\partial x} = 0 \tag{138}$$

where $\dot{x} \equiv \mathrm{d}x(s)/\mathrm{d}s$. Introducing (137) into (138) and solving the differential equation, one has $x(s) = -xs/t + x$, where the conditions $x(0) = x$ and $x(t) = 0$ must be taken into account. The Langrangian is then $L = -Mc^2\sqrt{1-(1/c^2)(x/t)^2} - V$ and from equation (136)

$$G(x,t) = -Mc^2 t\sqrt{1-\frac{1}{c^2}\left(\frac{x}{t}\right)^2} - Vt. \tag{139}$$

The position of the front is given by the condition $G(x,t) = 0$, that is $x = vt$ where

$$v = c\sqrt{1-\frac{V^2}{M^2c^4}} = 2\frac{\sqrt{Dk}}{1+\tau k} \tag{140}$$

which is the same speed, with proper units, as that derived by other methods (equations (79), (93) and (126)). The maximum value for the speed of the front is $v_{\max} = \sqrt{D/\tau}$, because it corresponds to the speed of light in the Hamilton–Jacobi equation. This upper bound was also derived for the linear analysis (equation (81)). The maximum speed may be reached for the case $k\tau = 1$, so the expression for the speed v (140) holds for $k\tau < 1$. This restriction was also required in the linear analysis (equation (82)).

The method presented in this subsection has been developed by Fedotov [49,51] and has been extended to nonuniform reaction rates [52,53], several dimensions [52] and anisotropic diffusion [54].

3.5. Approximate variational approach

We have shown in section 3.3 that the speed of fronts described by equation (9) satisfy the variational principle (105). As we will show in the applications section 4, for some source functions $f(n)$ the upper and lower bounds are different. Then, the approximate approach presented below gives better results for the speed [55]. The function g for which the right-hand side of equation (105) reaches its maximum satisfies equation (98),

$$(1-ac^2)hp = \frac{fg}{p}. \tag{141}$$

In the limit $n \to 1$ one has, since $n_{zz} \ll n_z$, $-c(1-af')p + f(n) \simeq 0$. This is an approximate relationship, so we may introduce α such that [55]

$$p = \frac{f(n)}{\alpha(1-af')} \simeq \frac{n(1-n)}{\alpha(1-af')}, \tag{142}$$

where the prime symbol denotes $' \equiv \mathrm{d}/\mathrm{d}n$. Therefore, equation (105) may be written as

$$\frac{c}{\sqrt{1-ac^2}} \simeq \max_{\alpha\in\mathcal{D}}\left[2\alpha\frac{\int_0^1 gf[(1-af')/(n(1-n))]\,\mathrm{d}n}{\int_0^1 g(1-af')\,\mathrm{d}n}\right], \tag{143}$$

where by integrating equation (141)

$$g(n) = \exp\left[-\frac{\alpha^2}{1-ac^2}\int f\frac{(1-af')^2}{n^2(1-n)^2}\,\mathrm{d}n\right], \tag{144}$$

and $\mathcal{D}$ is the set of values for α such that the above integrals exist. This method is very useful for source functions $f(n)$ such that the previous approaches break down or yield less precise results [55] (an explicit example will be presented in section 4.4). It has been also successfully applied to non-delayed equations, such as anomalous diffusion fronts in reactive systems and reaction–diffusion under advection [55].

3.6. Renormalization group technique

The renormalization group theory for wavefronts finds out approximate speeds assuming a small perturbation to an evolution equation the exact speed and front shape of which is known [41,55]. Consider a system described by the abstract equation $\partial_t n = N\{n\}$ and $n_0(z)$, $z = x - c_0 t$ is a stable travelling front solution with speed c_0. On the other hand, $n(z)$ is solution of the perturbed equation $\partial_t n = N\{n\} + \delta N\{n\}$. Its speed may be written as

$$c \simeq c_0 + \delta c, \tag{145}$$

where [41]

$$\delta c = -\frac{\int_{-\infty}^{\infty} \mathrm{d}z\, \varphi(z)[\mathrm{d}n_0/\mathrm{d}z]\delta N\{n_0\}}{\int_{-\infty}^{\infty} \mathrm{d}z\, \varphi(z)[\mathrm{d}n_0/\mathrm{d}z]^2}, \tag{146}$$

with $\varphi(z)$ an appropriate weight function, which we may take equal to $\mathrm{e}^{c_0 z}$. For equation (9), we shall treat a as a small perturbation [56]. The unperturbed equation is then $\partial_t n_0 = \partial_{xx} n_0 + f(n_0)$, whose exact solution $n_0(z)$ and speed c_0 must be known. Therefore,

$$\delta N\{n_0\} = -a f'(n_0) c_0 \frac{\mathrm{d}n_0}{\mathrm{d}z} - a \frac{\mathrm{d}^2 n_0}{\mathrm{d}z^2} c_0^2 \tag{147}$$

and introducing equation (147) in (146), one finds an approximate value for the speed c. We shall calculate it explicitly for a specific application in section 4.4.

4. Some applications of single-species models

PRD equations have been studied for more than 60 years [1, 29]. During this time, many important applications have been found, including the spread of advantageous genes [1, 57], population dynamics [57,28], the development of epidemics [4], nerve conduction [58], cellular sensitivity [59] and other biological phenomena, in addition to physical applications such as the spread of flames [29,2], superconductors [60], solidification [61], liquid crystals [62] and chemically reacting systems [18]. HRD equations have a comparatively much shorter history [33] and, as happened in the first applications of PRD equations, have for the moment been applied to many biological and some physical processes. This is reasonable since, as we shall see, HRD equations have been used to describe properly several experimental biophysical results which were previously unexplained. Also, the value of the delay time in equation (9) is relatively simple to estimate in such systems. In this section we select a wide variety of source functions which have relevant physical and biological applications, and apply the methods from section 3 to determine the speed of wavefronts. The way parameters are estimated from experimental data and direct comparison to observations is deferred to sections 6–8.

4.1. Logistic growth

The logistic source term (65) is

$$F(n) = An - Bn^2. \tag{148}$$

This is a realistic function driving the reproduction of many species [38]. We introduce dimensionless variables according to equations (69)–(72), choosing

$$\frac{1}{k} = \frac{1}{A} \tag{149}$$

for the reactive characteristic time. Then,

$$f(n) = n\left(1 - \frac{B}{A}n\right), \tag{150}$$

which satisfies the condition $f'(0) \neq 0$, is continuous and has $f'' < 0$. Whereas the linear analysis gives only the lower bound (79), the variational results (112) and (125) show that the asymptotic speed of the fronts is

$$c = \frac{2}{1+a}. \tag{151}$$

It should be recalled that c is a dimensionless speed. The true speed must be computed from equation (74), which yields

$$v = \frac{2\sqrt{DA}}{1+\tau A}. \tag{152}$$

Equation (151) is in agreement with the Hamilton–Jacobi method, equation (140), and also with MSA, equation (93). If the effect of the delay time is neglected ($a = \tau k = 0$), we recover the well-known result $c = 2$ or $v = 2\sqrt{DA}$ [1, 29, 39].

Equation (73) was solved numerically for the logistic source function in order to determine the speed of fronts for different values of a. The results of the simulations are compared to the analytical expression $c = 2/(1+a)$ in figure 2. The numerical simulations of equation (73) were performed [43] by assuming that initially $n = 1$ in a localized region and $n = 0$ elsewhere, and making use of the splitting operator technique [63]. The profile $n(x)$ was plotted at different times. By using the method in figure 1, one may then determine the asymptotic speed selected by the smooth front that is observed after an initial transient. From figure 2, it is seen that the simulations of hyperbolic wavefronts yield rather satisfactory agreement between the numerical results and equation (151). This equation will in turn be used in section 6 to compare to experimental observations.

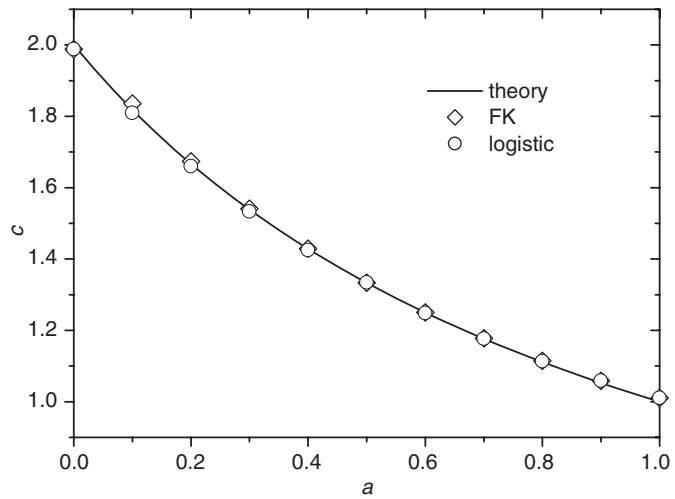

Figure 2. Comparative plot between the analytical expression for the dimensionless speed $c = 2/(1+a)$ and the dimensionless speed obtained from numerical integration of (73) as a function of the dimensionless parameter a for logistic growth (○) and generalized FK kinetics, $p = 2$ (◇) [43]. There is good agreement between numerical and analytical results.

4.2. Generalized Fisher–Kolmogorov kinetics

The logistic function is the simplest one leading to some reasonable results [38], such as the saturation of populations with a limited amount of available resources (see the text following equation (67)). However, other source functions are important in biological applications. A particularly relevant case is the Fisher–Kolmogorov (FK) source function, namely $f(n) = n(1 - \alpha n^2)$, which is important in genetics [1]. Here we will assume a generalized FK function,

$$f(n) = n(1 - \alpha n^p), \tag{153}$$

with $p \geqslant 1$. As in the logistic case, we have $f'(0) \neq 0$, f is continuous and $f'' < 0$. Thus using the variational results (112) and (125), we can predict the speed of wavefronts without any uncertainty, $c = 2/(1 + a)$. The Hamilton–Jacobi method also provides this result. It means that this expression for the selected speed holds not only for the logistic case, but also for more general situations of practical interest. From figure 2 [43], we see that this prediction agrees with the simulations of equation (73) for the FK source function.

4.3. HRD generalization of a cubic PRD model

Consider next the cubic source function

$$f(n) = \frac{n}{b}(1 - n)(b + n), \tag{154}$$

with $0 < b < 1$. This function has been applied in several reaction–diffusion studies on genetics, among them in the description of inferior heterozygotes selection [64] and of the morphogenetic field of a multicellular ensemble [65]. The source function (154) has also been useful because it can be solved exactly when the delay time is not accounted for ($a = 0$) [42,47].

A lower bound for the speed of fronts can be obtained form equation (112), namely, $2/(1+a)$. On the other hand, the source term (154) satisfies that $f'' < 0$ for $(1-b)/3 < n < 1$, but has $f'' > 0$ for $0 < n < (1 - b)/3$, so the upper bound (151) cannot be applied and we cannot obtain the exact asymptotic speed. However, we shall see that it is possible to constraint the speed. Let us first obtain a better lower bound. As in the case of PRD equations with the source term (154) [47], we choose $g(n) = (1 - n)^{2+2b} n^{-2b}$. We now apply the variational analysis method (section 3.3.1) for this single trial function instead of the sequence $g(n) = n^{\alpha-1}$. Equation (105) yields, after some algebra,

$$\frac{c}{\sqrt{1 - ac^2}} \geqslant 2 \frac{\dfrac{\sqrt{2b}}{\Gamma(4)} + \sqrt{\dfrac{2}{b}} \dfrac{1 - 2b}{\Gamma(5)}}{\dfrac{1 - a}{\Gamma(4)} + \dfrac{6a}{b} \dfrac{(1 - b)(1 - 2b)}{\Gamma(6)} - \dfrac{2a}{b} \dfrac{(1 - b)(1 - 2b)}{\Gamma(5)}}, \tag{155}$$

where the integrals have been solved making use of formula (3.191-3) in [48]—which applies under the assumption that $0 < b < 1/2$, $\Gamma(z)$ is the Gamma function and we have applied that $\Gamma(z + 1) = z\Gamma(z)$. From this we find the lower bound

$$c_{\mathrm{L}} = \begin{cases} c_{\mathrm{L}}(a, b), & 0 < b < \frac{1}{2} \\ \dfrac{2}{1 + a}, & \dfrac{1}{2} < b < 1 \end{cases}, \tag{156}$$

where

$$c_{\mathrm{L}}(a, b) = \frac{\sqrt{2b} + 1/\sqrt{2b}}{\sqrt{\left(1 - \dfrac{a}{5} \dfrac{1 + 2b + 2b^2}{b}\right)^2 + \dfrac{a}{2b} (1 + 2b)^2}}. \tag{157}$$

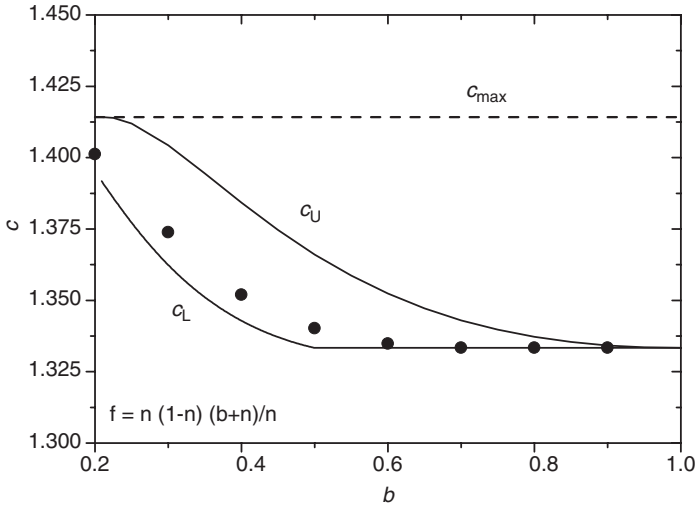

Figure 3. Comparative plot between lower and upper bounds for c and the results from simulations of equation (73) for the cubic source function (154). Here $a = 1/2$, and the range of values of b is constrained because of the range of validity of the variational approach. Lower and upper bounds are plotted in solid lines and numerical results in circles [43].

Notice that for $1/2 < b < 1$ the integrals in equation (105) diverge, so that we have resorted to the lower bound (112). In the PRD case ($a = 0$), we recover the result found by Ben-Jacob, namely $c_L = \sqrt{2b} + 1/\sqrt{2b}$ for $0 < b < 1/2$ and $2/(1 + a)$ for $1/2 < b < 1$ [42]. For the upper bound we cannot apply equation (125), as explained above, but we can still derive an upper bound from equations (122) and (154). Equation (122) yields, after some algebra,

$$\Phi(n) = \frac{1 + \frac{2}{b}n - 2n - \frac{3}{b}n^2 - a\left[1 + \frac{2(1-b)}{b}n + \frac{2(1-2b+b^2)}{b^2}n^2 - \frac{4(1-b)}{b^2}n^3 - \frac{3}{b^2}n^4\right]}{\left[1 - a\left(1 + \frac{2}{b}n - 2n - \frac{3}{b}n^2\right)\right]^3} \tag{158}$$

and the speed is given by equation (123). In the limit $b \to 1$, $f''(n) < 0$ and $\sup \Phi(n) = \Phi(0)$, thus $c_U \to 2/(1 + a)$. The variational analysis for the lower and upper bounds is restricted to the condition $1 - af' > 0$, which is equivalent to $a < M^{-1}$, with $M = \max_{n\in(0,1)} f'(n)$. For this case one finds $M = (1 + b + b^2)/3b$ and the restriction is $(5 - \sqrt{21})/2 < b < 1$ if $a = 1/2$. We have plotted the bounds for $a = 1/2$ in figure 3, as well as the results from numerical simulations of equation (73) with the source function (154), as a function of b. We observe good agreement between the simulations [43] and the lower and upper bounds. In this and the following cases, the MSA (section 3.2), Hamilton–Jacobi dynamics (section 3.4) and the linear approach (section 3.1) do not yield good results if one compares them with numerical simulations. This shows the usefulness of the variational method (section 3.3).

4.4. Forest fire models

HRD equations have been used to model the propagation of forest fires [16]. In this toy model, a direct relationship to experimental data is not pursued. However, it serves very

well to illustrate the application of the theory before attempting to apply it to explain several experimental results (sections 6–8). The reaction term considered is of the form

$$f(n) = n^{\beta}(1-n). \tag{159}$$

For $\beta = 1$, this reduces to the logistic case (section 4.1), so we will assume that $\beta > 1$. The parameter β quantifies the number of burning trees needed in order to set fire to a nearby, green tree [16]. For high values of β, it is expected intuitively that the speed of the fire front will be smaller.

4.4.1. Variational bounds. For equation (159), we have $f'(0) = 0$, thus the linear and MSA analysis (sections 3.1 and 3.2) do not hold. Therefore, we resort to the variational analysis (section 3.3). Still, since $f'(0) = 0$, equation (112) does not apply, and since $f'' < 0$ does not hold everywhere in (0,1) equation (125) cannot be applied either. As in section 3.3.1, let us consider the simple sequence of trial functions $g = n^{\alpha-1}$, with $0 \leqslant \alpha < 1$. The integrals in equation (105) are

$$\int_0^1 \sqrt{fgh}\,\mathrm{d}n = \sqrt{1-\alpha}\,\frac{\Gamma\left(\frac{\beta}{2}+\alpha-\frac{1}{2}\right)\Gamma\left(\frac{3}{2}\right)}{\Gamma\left(\alpha+1+\frac{\beta}{2}\right)}$$

$$\int_0^1 g(1-af')\,\mathrm{d}n = \frac{1}{\alpha} - a\frac{1-\alpha}{(\beta+\alpha)(\beta-1+\alpha)}. \tag{160}$$

Thus the best lower bound is given by

$$\frac{c_{\mathrm{L}}}{\sqrt{1-ac_{\mathrm{L}}^2}} = \max_{\alpha\in(0,1)}\{G(\alpha,\beta)\}, \tag{161}$$

where

$$G(\alpha,\beta) = \frac{2\alpha\sqrt{1-\alpha}\,\Gamma\left(\frac{\beta}{2}+\alpha-\frac{1}{2}\right)\Gamma\left(\frac{3}{2}\right)}{\Gamma\left(\alpha+1+\frac{\beta}{2}\right)\left[1-a\frac{(1-\alpha)\alpha}{(\beta+\alpha)(\beta-1+\alpha)}\right]}. \tag{162}$$

We have calculated the value of α which maximizes $G(\alpha,\beta)$ numerically for $a = 1/2$ and for different values of β between 1 and 7. The corresponding results for the lower bound c_{L} are plotted in figure 4.

For the upper bound we have to consider the function $\Phi(n)$, see equation (122). It reads

$$\Phi(n) = n^{\beta-2}\frac{\beta n - (\beta+1)n^2 - an^{\beta}[\beta+(\beta+1)n^2-2\beta n]}{(1-a[\beta n^{\beta-1}-(\beta+1)n^{\beta}])^3}. \tag{163}$$

We set, as for the lower bound, $a = 1/2$ and find the value n^* at which $\sup_{n\in(0,1)}\Phi(n) = \Phi(n^*)$ for different values of β between 1 and 7. For high values of β, $\Phi(n^*)$ must be computed numerically. The upper bound may be calculated finally from equation (121) or (123),

$$\frac{c_{\mathrm{U}}}{\sqrt{1-ac_{\mathrm{U}}^2}} = 2\sqrt{\Phi(n^*)}. \tag{164}$$

The results for the upper bound are plotted, together with the lower bounds and the numerical solution for the speed, in figure 4 for $a = 1/2$. The numerical solution is seen to lie between the upper and lower bounds, as it should, and it is a decreasing function with increasing values of β, as expected. One could certainly try other trial functions $g(n)$ and find other bounds. We have

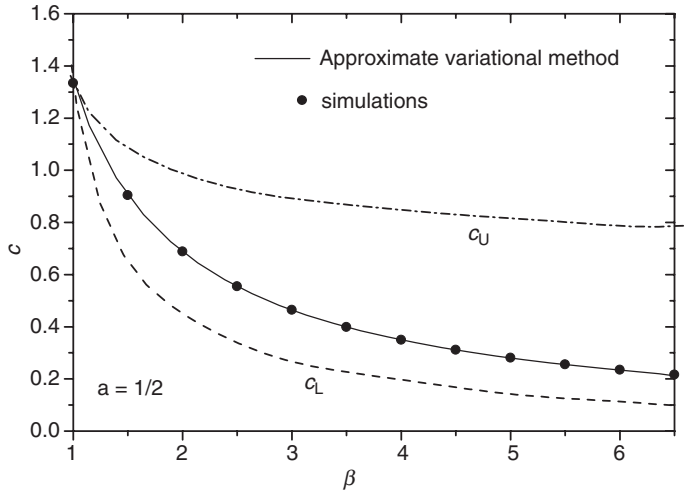

Figure 4. Forest fire models. Comparative plot between lower and upper dimensionless bounds, the approximated variational solution and the numerical integration of equation (73) for the dimensionless speed c of fire fronts as a function of parameter β, with $a = 1/2$. The numerical values [43] for the speed lie between both curves, as they should, but the approximated variational method fits very well with numerical solutions. As it is expected for forest fire models, the speed is a decreasing function for increasing values of β. The speed computed by means of the approximate variational method, equation (165), is shown as a full line [55].

used the same trial functions as in previous sections since they yield relatively simple results which illustrate fairly well the usefulness of the hyperbolic variational principle. It is also seen from figure 4 that the new upper bound c_U derived here is much better that $c_{max} = 1/\sqrt{a} = \sqrt{2}$ (see equation (106)).

4.4.2. Approximate variational method. At the beginning of this subsection we have mentioned that the linearization and MSA approaches (sections 3.1 and 3.2) cannot be applied to the case under consideration. This is why we have made use of the variational approach (section 3.3). The Hamilton–Jacobi method (section 3.4) does not hold in this case because the source term (159) does not fulfil the conditions (129). However, it is very interesting to show that the approximate variational method (section 3.5) yields a very good prediction for the speed as compared to numerical results [55].

For the source term (159), the approximate speed may be determined from equation (143)

$$\frac{c}{\sqrt{1-ac^2}} \simeq \max_{\alpha\in\mathcal{D}} \left\{ 2\alpha \frac{\int_0^1 g n^{\beta-1}[1-af']\,\mathrm{d}n}{\int_0^1 g[1-af']\,\mathrm{d}n} \right\}, \tag{165}$$

where from equation (144) one has

$$g = \exp\left(-\frac{\alpha^2}{1-ac^2} \int n^{\beta-2} \frac{[1-af']^2}{1-n}\,\mathrm{d}n \right), \tag{166}$$

and $f' \equiv \mathrm{d}f/\mathrm{d}n = \beta n^{\beta-1} - (1+\beta)n^{\beta}$. For illustration purposes, consider, e.g. the case $a = 1/2$. The integrals in equations (165) and (166) can be performed numerically, and from figure 4 it is seen that this result is more accurate than the bounds found above.

4.4.3. Renormalization group technique. Figure 4 corresponds to the case $a = 1/2$ and different values of β. In this case, it is not possible to apply the renormalization-group (RG) approach (section 3.6), because no exact solution $\rho(z)$ is known for arbitrary β. However, an exact solution exists for $\beta = 2$, a value for which the source function (159) has been applied to model the spread of microorganisms [66]. Thus, the RG method can be used to assess the results above [56]. Moreover, we shall see that it yields a much simpler and useful expression than the approximate result (165).

As explained in section 3.6, the RG approach can be applied by treating the reduced delay a as a smallness parameter, so that it introduces a small perturbation to the usual, non-delayed equation. Thus, we are treating the HRD equation (73) as a perturbation of the parabolic equation (68). This is indeed reasonable, because the HRD equation is a first-order approximation to the full time-delayed equation (see, e.g. section 2.1) and, on the other hand, the RG technique is nothing but a first-order approach to the problem $\partial_t \rho = N(\rho)$. The unperturbed equation for $\beta = 2$ is thus given by equations (73) and (159) with $a = 0$,

$$\partial_t \rho_0 = \partial_{xx} \rho_0 + \rho_0^2 (1 - \rho_0). \tag{167}$$

It is easily seen that this equation has a solution with the profile

$$\rho_0(z) = \frac{1}{1 + \mathrm{e}^{z/\sqrt{2}}}, \tag{168}$$

where $z = x - c_0 t$ and $c_0 = 1/\sqrt{2}$. The perturbation operator is easily found,

$$\begin{aligned} \delta N\{\rho_0\} &\equiv N\{\rho_0\} - N_{a=0}\{\rho_0\} \\ &= a[f'(\rho_0)\partial_t \rho_0 - \partial_{tt}\rho_0] \\ &= a\left[-c_0(2 - 3\rho_0)\rho_0 \frac{\mathrm{d}\rho_0}{\mathrm{d}z} - c_0^2 \frac{\mathrm{d}^2 \rho_0}{\mathrm{d}z^2}\right]. \end{aligned} \tag{169}$$

Then, by choosing the weight function $\varphi(z) = \mathrm{e}^{z/\sqrt{2}}$ we can perform the necessary integrations in equation (143), and equation (145) yields

$$c_{\mathrm{RG}} \simeq \frac{1}{\sqrt{2}} - \frac{\sqrt{2}}{40} a + \mathrm{O}(a^2). \tag{170}$$

In figure 5 we compare the results of numerical simulations of equations (23) and (159) with $\beta = 2$ to those from the approximate method (equation (165)), from the RG approach (equation (170)), and also with the lower and upper bounds derived above. In contrast to figure 4, in figure 5 we consider different values of the reduced delay a. The agreement of the approximate method with the numerical simulations is clear again. The speed decreases for increasing delay time, as was to be expected intuitively. It is not surprising that the RG approach becomes less reliable at higher delays, whereas the approximate method does not, since the RG approach is a first-order approximation valid only for small enough delays (see equation (170)). However, the RG technique is rather appealing because it gives a simple result (equation (170)) that is much more easy and practical to handle than that of the approximate method (equations (165) and (166)). Let us stress, however, that the RG approach cannot be applied for arbitrary β, because of the lack on an exact solution $\rho_0(z)$. Then, one must resort to the approximate approach presented above.

4.5. Bistable systems

In several problems arising in biology (nerve conduction [67]) and physics (electrothermal instability [68, 69]), it is found that the source term is given by

$$f(n) = n(1 - n)(n - \sigma) \qquad \text{for } 0 < \sigma < 1. \tag{171}$$

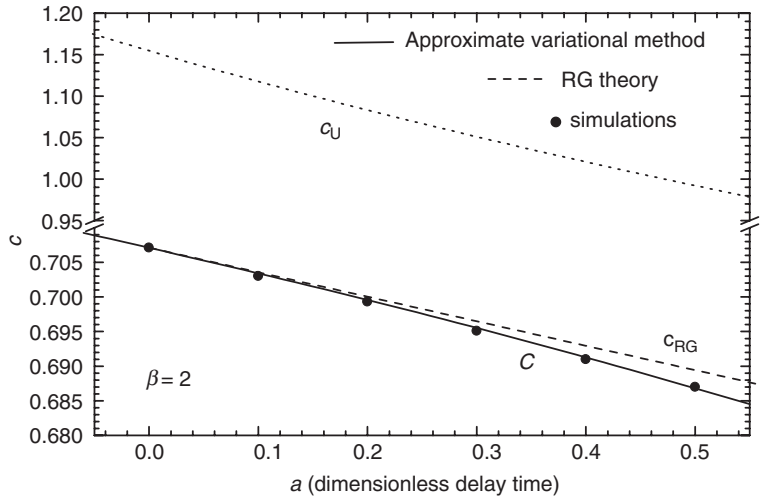

Figure 5. Time-delayed front speed c for forest fires as a function of the dimensionless delay time a. Dots are from numerical simulations [55]. The full line is the approximate prediction (165), whereas the dashed one is the RG prediction (170). The dotted line is the upper bound. The lower bound (not shown) yields $c > 0.46$.

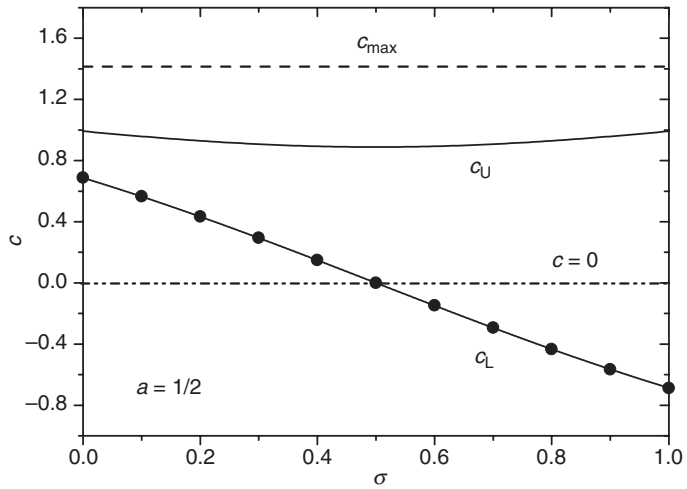

Figure 6. Bistable systems. Comparative plot between lower and upper bounds and the numerical solution for the dimensionless speed of fronts c for (equation (171)), with $a = 1/2$ [43]. Note the change of sign for the speed at $\sigma = 1/2$.

In these cases the system is called bistable. The reason is the following: the parameter σ has a critical value $\sigma = 1/2$ for which the stability of the states $n = 0$, 1, is inverted and the front changes its direction of propagation. For $\sigma < 1/2$ the front connects $n = 0$ to $n = 1$ and $c > 0$, for $\sigma = 1/2$ we have $c = 0$ and finally, for $1/2 < \sigma < 1$ the front connects $n = 1$ to $n = 0$ and $c < 0$. This can be seen in figure 6. Bounds for the speed can be derived [43] by using the variational method (section 3.3) and choosing the trial function $g(n) = (1 - n)^{2-2\sigma} n^{2\sigma}$, as in the cubic HRD model (section 4.3). By following the same steps as in previous sections, one

now obtains obtain the following lower bound

$$c_{\mathrm{L}} = \frac{1-2\sigma}{\sqrt{2[1-(a/5)(1-2\sigma+2\sigma^2)]^2 + a(1-2\sigma)^2}}, \tag{172}$$

which holds for any $\sigma \in (0,1)$. Similarly, one may derive the upper bound analytically, although it is extremely complicated and we prefer to present it graphically: figure 6 shows the lower and upper bounds for $a = 1/2$, as well as the speed obtained from numerical simulations of equations (73) and (171) [43]. According to figure 6, the upper bound from the variational method is again better than the bound $c_{\max} = 1/\sqrt{a} = \sqrt{2}$ (equation (106)). It is worth to note that in this case there is excellent agreement between the lower bound and the numerical solution. In figure 6 we also observe the change of sign for the speed at $\sigma = 1/2$. The restriction for the validity of the variational method $a < M^{-1}$ for $M = \max_{n\in(0,1)} f'(n)$ yields to $a < 3/(\sigma^2 - \sigma + 1)$, which imposes no additional restriction for $a = 1/2$.

4.6. Thermal wavefronts

Although in this review we focus our attention in reaction–diffusion systems, it is worth to summarize some closely related work which applies to reaction–conduction systems. In such cases, the main phenomena in the system are conductive energy transfer and a chemical reaction with a nonnegligible reaction heat. Then, several authors have argued for the use of the thermal equivalent of equation (9),

$$\rho c_{\mathrm{e}}\left(\frac{\partial T}{\partial t} + \tau\frac{\partial^2 T}{\partial t^2}\right) = \lambda\frac{\partial^2 T}{\partial x^2} + F(T) + \tau\frac{\partial F(T)}{\partial t} - \left[F(T) + \tau\frac{\partial F(T)}{\partial t}\right]_{T=T_0}, \tag{173}$$

where T is the temperature, ρ the density, c_{e} the specific heat (per unit mass), λ the thermal conductivity and

$$F(T) = Q v_{\mathrm{ch}}(T) \tag{174}$$

is the reaction heat Q times the reaction rate $v_{\mathrm{ch}}(T)$. equation (173) can be derived, e.g. by considering equation (6) instead of (7) and repeating the derivation in section 2.3. The last term in equation (173) is introduced to solve the so-called cold boundary problem [2,44], with T_0 the room, initial temperature which, in this way, corresponds to an equilibrium state of the system. This term is unimportant at higher temperatures, e.g. at the flame temperature in combustion fronts, because of the exponential dependence of the reaction rate, which for some combustion waves is given by a law of the Arrhenius form, e.g.

$$v_{\mathrm{ch}}(T) = An\exp\left[-\frac{E_{\mathrm{a}}}{kT}\right], \tag{175}$$

where A is the activation energy, n the fuel concentration (with $n \simeq n_0$ at the leading edge of the front), E_{a} the activation energy, k Boltzmann's constant and T the absolute temperature.

It is easy to apply the linearization analysis in section 2.1 to equation (173), yielding [21]

$$v \geqslant v_{\mathrm{L}} = \frac{2\sqrt{\lambda Q(\partial v_{\mathrm{ch}}/\partial T)|_{T=T_0}}}{\rho c_{\mathrm{e}} + \tau Q(\partial v_{\mathrm{ch}}/\partial T)|_{T=T_0}}. \tag{176}$$

If the relaxation time can be neglected (Fourier or classical heat conduction, $\tau \to 0$), this reduces to

$$v_{\mathrm{L}} = \frac{2}{\rho c_{\mathrm{e}}}\sqrt{\lambda Q\left.\frac{\partial v_{\mathrm{ch}}}{\partial T}\right|_{T=T_0}}, \tag{177}$$

which is the KPP result (see [29] and [2], p 281). Note that

$$\tau_{\mathrm{r}} \equiv \frac{\rho c_{\mathrm{e}}}{Q(\partial v_{\mathrm{ch}}/\partial T)|_{T=T_0}} \tag{178}$$

has units of time and may be seen as a characteristic timescale of the reactive process. Thus

$$v_{\mathrm{L}} \sim \sqrt{\frac{\chi}{\tau_{\mathrm{r}}}}, \tag{179}$$

with $\chi \equiv \lambda/\rho c_{\mathrm{e}}$ the thermal diffusivity. This agrees with the estimation for the speed of flames derived by Landau [70] on the basis of the propagation of heat disturbances according to the classical equation of heat transfer [71]. On the other hand, use of the Arrhenius law (175) into equation (177) yields

$$v_{\mathrm{L}} = \frac{2\sqrt{\lambda Q A n_0 E_{\mathrm{a}}/k}}{\rho c_{\mathrm{e}} T_0} \exp\left[-\frac{E_{\mathrm{a}}}{2kT_0}\right]. \tag{180}$$

Recall that this gives a lower bound only. Simulations show that it agrees with the selected speed v for low chemical to thermal energy ratios E_{a}/kT [44]. Some open problems that deserve future attention are the application of the time-delayed solution (176) to (i) combustion fronts in which the delay time τ takes care of the ignition delay that is observed experimentally [72], and (ii) more realistic forest fire models (see section 4.4) in which the delay time is related to the time needed to ignite a green tree [16, 73].

An equation of the type of (173) has been also applied to analyse the thermal behaviour of a superconductor device that presents electrothermal instability. In this application, one considers an equation for the dimensionless temperature $\tilde{T}$ of the form

$$\frac{\partial \tilde{T}}{\partial t} + \tau \frac{\partial^2 \tilde{T}}{\partial t^2} = D\frac{\partial^2 \tilde{T}}{\partial x^2} + F(\tilde{T}) + \tau \frac{\partial F(\tilde{T})}{\partial t} \tag{181}$$

with a piecewise linear reaction term

$$F(\tilde{T}) = \omega[-\tilde{T} + \theta(\tilde{T} - \tilde{T}^*)], \tag{182}$$

which approximately accounts for heat losses to the bath and the Joule effect in a superconducting wire (θ is the Heaviside step function and $\tilde{T}^*$ the dimensionless critical temperature) [74, 75, 68]. For this specific source term, it has been possible to derive an explicit solution by means of Fourier transforms, yielding the front speed [74]

$$c = -\frac{2}{\sqrt{\omega D}} \frac{1 - 2\tilde{T}^*}{(1+\omega\tau)\sqrt{1-(1-2\tilde{T}^*)^2}}. \tag{183}$$

Note that this is a thermal example of bistable system (section 4.5), because the sign of c depends on the value of $\tilde{T}^*$ [75]. For $\tau \to 0$, one recovers the classical result [75]. Méndez and Compte have proposed a particular system where an experimental check of equation (183) could be made: a Ballast resistor consisting of a superconducting wire carrying a constant current and surrounded by a cold heat bath at a temperature lower than that of the superconductor. By keeping one end of the wire at a constant temperature higher than the critical one and the other end at the bath temperature, if hyperbolic heat transport applied then the observed front speed would be different than that predicted by the classical theory [74].

Galenko and Danilov [19, 20] have considered a time-delayed equation with the form of equation (173),

$$\rho c_{\mathrm{e}}\left(\frac{\partial T}{\partial t} + \tau \frac{\partial^2 T}{\partial t^2}\right) = \lambda \frac{\partial^2 T}{\partial x^2} + F(T) + \tau \frac{\partial F(T)}{\partial t} \tag{184}$$

with the source term (174)

$$v_{\mathrm{ch}}(T) = \delta(T - T_Q), \tag{185}$$

with δ the Dirac delta, to describe fast solidification fronts. Then, Q appearing in equation (174) is the solidification heat per unit volume and T_Q the solidification temperature at which the phase transition occurs. In this framework, one may derive the solidification front speed as a function of the initial supercooling in the system [19]. In their very recent work, Galenko and Danilov find a discrepancy (at high supercoolings) of about 8% relative to the classical predictions ($\tau \to 0$) by using known parameter values for the solidification of pure Nickel. Experimental values refer to needle-like crystals or dendrites, so that the simple 1D model summarized above is not realistic. This will require models with several dimensions and this is an interesting area which deserves further study.

5. HRD equations for several species

Consider a system with two variables n and m undergoing reaction–diffusion dynamics ([43], section 5.1). In biological applications, they may represent the predator and prey population densities [28], those of farmers and hunter-gatherers in the expansion of agricultural communities [57], of the infected and susceptible individuals in the spread of a pandemic [1], etc. Such systems of equations are called Lotka–Volterra equations. Two-variable systems are also important in the propagation of domain walls in superconductors: then n corresponds to the superconducting order parameter, m to the gauge-invariant vector potential and they follow Ginzburg–Landau equations [60] which have in fact the same mathematical form of Lotka–Volterra equations.

Let us consider the system of two species

$$\begin{cases} \tau n_{tt} + n_t = Dn_{xx} + F(n) + \tau F'(n) n_t + \gamma nm, \\ \hat{\tau} m_{tt} + m_t = \hat{D} m_{xx} + \hat{F}(m) + \hat{\tau} \hat{F}'(m) n_t - \hat{\gamma} nm, \end{cases} \tag{186}$$

which is a pair of coupled HRD equations (see equation (9)). The superscript $\hat{}$ refers to the species with number density m, and the last term in these equations corresponds to the interaction between both species. This simple term means that in, for example, a predator–prey system with $\tau = \hat{\tau} = 0$, the predators increase their population density n because of their interaction with preys, which in turn experience a decrease in their population density m. It should be emphasized that here we are assuming that the interaction rate γnm is small compared to the other terms, since otherwise higher-order terms in $n^2 m$, etc could be important in the description of the interaction among both species. For $\tau = \hat{\tau} = 0$ we recover the usual (or PRD) Lotka–Volterra system with spatial inhomogeneities (see chapter 12 in [28]). The wavefront speed problem for equations (186) has been tackled [43] by extending the linear and variational theories in section 3 in the present review. As said above, we consider HRD equations, thus the results applying to PRD equations will follow in the limit $\tau \to 0$. In order to illustrate our procedure, let us consider for a moment a specific problem (which will be analysed in more detail in sections 6 and 7): in the neolithic transition, the population wavefronts of farmers (with number density n) traveled into areas where they encountered a population of preexisting hunter-gatherers with a number density m that is usually assumed to be approximately uniform, say m_0 [57,76]. Both populations mixed to some extent, and this interaction is regarded as the cause of the gradients observed in the present spatial distribution of human genes [57]. We may describe the process by following exactly the same procedure as in section 2 but making use of the coupled equations (186) instead of equation (9): the procedure is essentially the same as in section 3, so we shall only give the main steps. Since the problem we have in mind

is the expansion of, say, farming communities, we consider the corresponding equation in the leading edge of the front ($n \approx 0$),

$$(1 - ac^2)\epsilon_{zz} + c[1 - af'(0)]\epsilon_z + [f'(0) + \tilde{\gamma}m_0]\epsilon = 0, \tag{187}$$

where $\tilde{\gamma} = \gamma/k$, and the rest of the notation is the same as in section 3. This equation generalizes equation (76) and is decoupled from the evolution equation of species m. Note that we cannot apply equation (79) with $f'(0) + \gamma m_0$ instead of $f'(0)$, because the parentheses multiplying ϵ_z in equation (187) does not contain $f'(0) + \gamma m_0$ but only $f'(0)$, thus equation (187) does not have the same form as equation (76). But it is clear that, as in section 3.1, the asymptotic solutions near $n = 0$ are given by equation (78), with $\lambda_\pm$ the solution to the characteristic equation, which now reads

$$(1 - ac^2)\lambda^2 + c[1 - af'(0)]\lambda + f'(0) + \tilde{\gamma}m_0 = 0. \tag{188}$$

As in section 3.1, we require $\mathrm{Im}(\lambda) = 0$ in order to prevent the solution from oscillating. This yields

$$c \geqslant 2\sqrt{\frac{f'(0) + \tilde{\gamma}m_0}{[1 + af'(0)]^2 + 4a\tilde{\gamma}m_0}}. \tag{189}$$

This result reduces, as it should, to the lower bound (79) for noninteracting species ($\tilde{\gamma} = 0$). On the other hand, in the absence of a delay time τ (i.e. $a = \tau k = 0$) we obtain

$$c \geqslant 2\sqrt{f'(0) + \tilde{\gamma}m_0}, \tag{190}$$

and if we assume that both the effect of the interaction and that of the delay are negligible, we recover the Fisher–KPP result for PRD equations, namely $c \geqslant 2\sqrt{f'(0)}$. Equation (190) could have been obtained simply from the fact that in the non-delayed (or PRD) model $\tau = 0$ the first equation (186) is nothing but a PRD equation with $f(n) + \gamma nm$ instead of $f(n)$, and we have assumed that $m \approx m_0$ near $n = 0$. The PRD limit (190) agrees with previous research, where it has been applied to predator–prey systems (see equation (12.10) in [28]; see also [77]) and to the propagation of interfaces in superconductors[3].

It should be noted that equation (189) provides just a lower bound, simply because it is based on the linear approach (section 3.1). We now make use of the variational approach to HRD equations (section 3.3). First of all we note that we cannot make use of equation (125) with $f'(0) + \gamma m_0$ instead of $f'(0)$, because the evolution equation corresponding to the first equation (186) is

$$(1 - ac^2)n_{zz} + c[1 - af'(n)]n_z + f(n) + \tilde{\gamma}m_0 n = 0, \tag{191}$$

and this is not reducible to an equation of the type of (73) since $(f(n)+\tilde{\gamma}m_0 n)' = f'(n)+\tilde{\gamma}m_0 \neq f'(n)$. Thus we have to generalize the approach in section 3.3. Since the steps are exactly the same as there, it will suffice to sketch the derivation. Equation (94) is generalized into

$$(1 - ac^2)p\frac{\mathrm{d}p}{\mathrm{d}n} - c[1 - af'(n)]p + f(n) + \tilde{\gamma}m_0 n = 0. \tag{192}$$

We multiply this by g/p, with $p \equiv -n_z$ and $g > 0$, and integrate by parts. As before, $h = -g' > 0$ and we apply the general inequality $(r + s) \geqslant 2\sqrt{rs}$ to get rid of p. This finally yields

$$\frac{c}{\sqrt{1 - ac^2}} \geqslant 2\frac{\int_0^1 \sqrt{(f(n) + \tilde{\gamma}m_0 n)gh}\,\mathrm{d}n}{\int_0^1 g(1 - af'(n))\,\mathrm{d}n}, \tag{193}$$

[3] Note the different units and the minus sign in that equation, which arises because of the minus sign in the term $-q^2 f$ in equation (2) in this reference q^2, Q_∞^2 and f in this reference correspond to $\tilde{\gamma}m$, $\tilde{\gamma}m_0$ and n here, respectively, and we have considered the case of small reduced interaction rate $\tilde{\gamma}m_0$ (small values of Q_∞^2 in [60]) since otherwise the interaction rate would be fast enough to modify m and n in very short timescales; thus the approximation $m \approx m_0$ would break down even in the leading edge of the front (i.e. near $n = 0$).

which generalizes equation (97).

We can now derive lower and upper bounds from the variational analysis. If we consider again the trial functions $g = n^{\alpha-1}$, equation (193) becomes

$$\frac{c}{\sqrt{1-ac^2}} \geqslant 2\sqrt{1-\alpha}\,\frac{\int_0^1 n^{\alpha-3/2}\sqrt{(f(n)+\tilde{\gamma}m_0 n)}\,\mathrm{d}n}{\int_0^1 n^{\alpha-1}[1-af'(n)]\,\mathrm{d}n}. \tag{194}$$

In the limit $\alpha \to 0$, the integrands diverge at $n = 0$, thus only the singular point will contribute. We expand the integrands in Taylor series near $n = 0$, and only the leading term in the expansions will survive. Thus, assuming $f'(0) \neq 0$,

$$\frac{c}{\sqrt{1-ac^2}} \geqslant 2\sqrt{1-\alpha}\,\frac{\int_0^\varepsilon n^{\alpha-3/2}\sqrt{f'(0)n+\tilde{\gamma}m_0}\,\mathrm{d}n}{\int_0^\varepsilon n^{\alpha-1}[1-af'(0)]\,\mathrm{d}n}. \tag{195}$$

Performing the integrals and taking the limit $\alpha \to 0$ we obtain

$$c \geqslant c_{\mathrm{L}} = 2\sqrt{\frac{f'(0)+\tilde{\gamma}m_0}{[1+af'(0)]^2+4a\tilde{\gamma}m_0}}, \tag{196}$$

in agreement with the result (189) from the linear analysis. Thus also for interacting species, the linearization and variational methods yield the same lower bound. We now derive upper bounds. Since the only change of equation (193) relative to (97) is that $f + \tilde{\gamma}m_0 n$ appears instead of f, we define $\mu(n)$ and $\alpha(n)$ performing this change in the corresponding definitions in section 3.3.2, i.e. $\mu(n) = g[1 - af']$ as before and $\alpha(n) = (f + \tilde{\gamma}m_0 n)h/[g(1 - af')^2]$. We have then, from equations (193) and (113),

$$\frac{c}{\sqrt{1-ac^2}} \leqslant 2\max_g \left[\frac{\int_0^1 [(f+\tilde{\gamma}m_0 n)h/(1-af')]\,\mathrm{d}n}{\int_0^1 g(1-af')\,\mathrm{d}n}\right]^{1/2}. \tag{197}$$

We integrate by parts,

$$\int_0^1 \frac{(f+\tilde{\gamma}m_0 n)h}{1-af'}\,\mathrm{d}n = -\frac{g(1)\tilde{\gamma}m_0}{1-af'(1)} + \int_0^1 g\left(\frac{f'+\tilde{\gamma}m_0}{(1-af')^2} + \frac{af''(f+\tilde{\gamma}m_0 n)}{(1-af')^3}\right)\mathrm{d}n. \tag{198}$$

We note that, in contrast to what happened in the case of a single species (equation (119)), the boundary term does not vanish. But recalling that $g > 0$ and the condition $1 - af' > 0$ we have

$$\int_0^1 \frac{(f+\tilde{\gamma}m_0 n)h}{1-af'}\,\mathrm{d}n \leqslant \int_0^1 g\left(\frac{f'+\tilde{\gamma}m_0}{(1-af')^2} + \frac{af''(f+\tilde{\gamma}m_0 n)}{(1-af')^3}\right)\mathrm{d}n, \tag{199}$$

and, in order to get an upper bound independent of g,

$$\int_0^1 \frac{(f+\tilde{\gamma}m_0 n)h}{1-af'}\,\mathrm{d}n \leqslant \sup_{n\in(0,1)}\left[\frac{f'+\tilde{\gamma}m_0}{(1-af')^2} + \frac{af''(f+\tilde{\gamma}m_0 n)}{(1-af')^3}\right]\int_0^1 g(1-af')\,\mathrm{d}n. \tag{200}$$

Thus,

$$\Phi(n) \equiv \frac{f'+\tilde{\gamma}m_0}{(1-af')^2} + \frac{af''(f+\tilde{\gamma}m_0 n)}{(1-af')^3}. \tag{201}$$

If we assume that the source function f is continuous and that $f'' < 0$, after recalling again the condition $1 - af' > 0$, we see that the second term in $\Phi(n)$ is negative (it only vanishes at $n = 0, 1$), whereas the first term decreases for increasing values of n. Thus,

$$\sup_{n\in(0,1)} \Phi(n) = \frac{f'(0)+\tilde{\gamma}m_0}{(1-af'(0))^2}, \tag{202}$$

and we have the simpler result

$$c \leqslant c_{\mathrm{U}} = 2\sqrt{\frac{f'(0) + \tilde{\gamma} m_0}{[1 + af'(0)]^2 + 4a\tilde{\gamma} m_0}}, \tag{203}$$

which reduces to equation (125) in the limit $\tilde{\gamma} \to 0$, as it should, and holds provided that f is continuous and concave in (0, 1). Under these assumptions, our upper bound is the same as the lower one (196) and the asymptotic speed of the fronts for interacting species can also be predicted without any uncertainty,

$$c = 2\sqrt{\frac{f'(0) + \tilde{\gamma} m_0}{[1 + af'(0)]^2 + 4a\tilde{\gamma} m_0}}. \tag{204}$$

If the delay time is not taken into account (PRD approach, $a = 0$), this reduces to

$$c = 2\sqrt{f'(0) + \tilde{\gamma} m_0}, \tag{205}$$

in agreement to previous work ([77] and footnote 3) . Figure 7 is a comparison of the analytical result (205) for the expansion of species n with numerical integrations for the case $\tau = 0$. The numerical integrations were performed [43] by assuming that initially $n = 1$ in a localized region and $n = 0$ elsewhere, and $m = m_0$ everywhere; the equations used are (186) in the same variables as equation (73), i.e.

$$\begin{aligned} an_{tt} + n_t &= n_{xx} + f(n) + af'(n)n_t + \tilde{\gamma} n m_0, \\ \hat{a} m_{tt} + m_t &= m_{xx} + \hat{f}(m) + \hat{a}\hat{f}'(m)m_t + \hat{\tilde{\gamma}} n m_0, \end{aligned} \tag{206}$$

where $\hat{a} = \hat{k}\hat{\tau}$, $\hat{\tilde{\gamma}} = \tilde{\gamma}/\hat{k}$ and, analogously to equation (73), $1/\hat{k}$ is a characteristic reactive time for species m. In the simulations we have assumed for definiteness that $\hat{a} = a$, $\hat{\tilde{\gamma}} = \hat{\gamma}$, as well as logistic growth functions, i.e. $f(n) = n(1 - n)$ and $\hat{f}(m) = m(1 - m)$. Figure 8 compares the predictions of equation (204) to the simulations of equations (206) for $\tau \neq 0$. There is

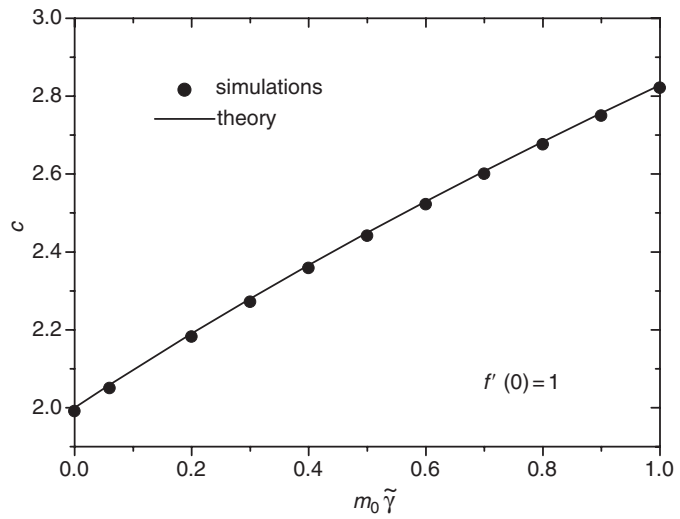

Figure 7. PRD Lotka–Volterra equations. Comparison between analytical results and numerical simulations for the dimensionless front speed c, as a function of the interaction parameter $\tilde{\gamma} m_0$ [43]. The dots are results from numerical simulations of equations (206) for the PRD case ($\tau = 0$) and $f'(0) = 1$. The solid line is prediction given by equation (205).

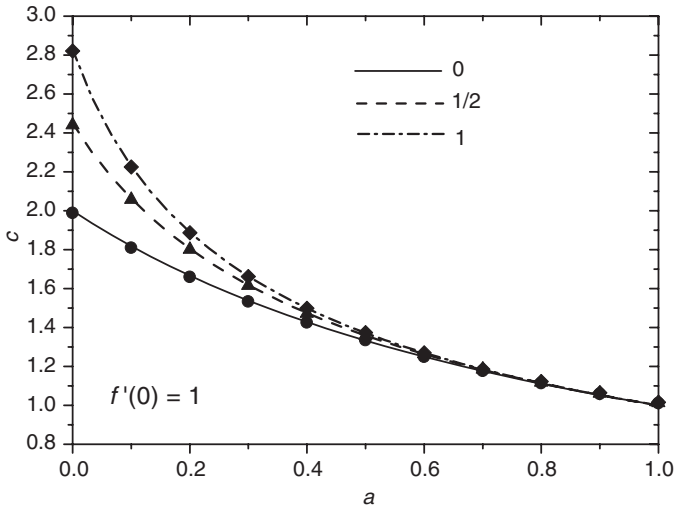

Figure 8. HRD (or time-delayed) Lotka–Volterra equations. Comparison between analytical results and numerical simulations for the dimensionless front speed c in , as a function of $a = \tau k$ (for $\tilde{\gamma} m_0 = 0$, $\tilde{\gamma} m_0 = 1/2$, and $\tilde{\gamma} m_0 = 1$) [43]. The symbols are results from numerical simulations of equations (206), and the curves are the predictions form equation (204). There is excellent agreement in all cases.

good agreement in both the classical (figure 7) and the time-delayed (figure 8) cases. By comparison to the results for $\gamma m_0 = 0$, it is also seen that the interaction among both species leads to a faster wavefront, as was to be expected since the last term in the first equation (186) corresponds to a numeric increase in the expanding species. This was conjectured in [22] and is why the front speed increases with increasing values of $\tilde{\gamma} m_0$. Comparison to observations is presented in section 7.

Before closing the topic of solutions to the front speed problem, let us mention that some authors have applied several-species HRD equations to thermal transport. Then, the role of the species concentrations n and m is played by the temperatures T and $\hat{T}$ of a two-component mixture. If the symbol ˆ refers to an inert component to which heat is transferred from the other component, the simplest analogues to equations (186) being

$$\begin{cases} \rho c_{\mathrm{e}}(\tau T_{tt} + T_t) = \lambda T_{xx} + F(T) + \tau F'(T) T_t - \alpha(T - \hat{T}), \\ \hat{\rho}\hat{c}_{\mathrm{e}}\hat{T}_t = -\alpha(T - \hat{T}), \end{cases} \tag{207}$$

where the last term in both equations corresponds to energy-relaxation process. For a single-temperature system, the first of these equations reduces to equation (173). Equations of the type of (207) have been applied by Qiu and Tien [78] and Sobolev [79] to laser heating of metals. Then, heat is mainly transported by electrons (temperature T), which lose energy to the lattice (temperature $\hat{T}$), and the source term $F(T)$ corresponds not to a chemical reaction but to a laser heat source. For combustion waves in a fuel diluted in an inert component, $F(T)$ has the Arrhenius form (174) and (175) and it is easily seen, in the same way as in the analysis in section 4.5, that the front speed satisfies [21]

$$v \geqslant \frac{2\sqrt{\lambda(Q(\partial v_{\mathrm{ch}}/\partial T)|_{T=T_0} - \alpha)}}{\rho c_{\mathrm{e}} + \tau(Q(\partial v_{\mathrm{ch}}/\partial T)|_{T=T_0} - \alpha)}. \tag{208}$$

which reduces to equation (176) for single-temperature systems. Recall that for parabolic, classical transport, that equation in turn reduces to the KPP (177) and Landau (179) results.

6. Comparison to experiment: single-species models

As mentioned at the beginning of section 3, HRD equations have a comparatively much shorter history than their PRD counterparts and, as happened in the first applications of PRD equations, have for the moment been applied essentially to biological processes. This is essentially due to the availability of observations which cannot be satisfactorily accounted for within the classical, PRD approach. Below we review some topics for which direct comparison of theoretical predictions to observational values has been already performed.

6.1. The neolithic transition in Europe

An interesting, direct application of the classical, PRD equation (12) arose after archaeological data lead to the conclusion that European farming originated in the Near East, from where it spread across Europe. The rate of this spread was measured [80], and a mathematical model was proposed according to which early farming expanded in the form of a PRD wave of advance [57]. Such a model provides a consistent explanation for the origin of Indo-European languages [81], and also finds remarkable support from the observed gene frequencies [82]. However, this PRD model predicts a velocity for the spread of agriculture that is higher than that inferred from archaeological evidence, provided that one accepts those values for the parameters in the model that have been measured in independent observations [57]. Here we will review an approach to this problem based on an HRD model [43].

In order to make comparison to experiment possible for this process, we need a more detailed microscopic model than those presented in section 2. Such a model should (i) apply to 2D spaces, (ii) provide a reasonable description of the microscopic motion of individuals (thus allow for 'jumps' of unequal length, in contrast to, e.g. the model in section 2.1) and (iii) relate the macroscopic parameters (τ and D) appearing in the HRD equation (9) (or, more precisely, the extension of (9), derived below) to the microscopic properties of the system, so that the values of τ and D can be estimated from the observations available. Such a model is presented below, and its predictions are compared to observations [22].

Let $p(x, y, t)$ stand for the population density (measured in number of families per square kilometre), where x and y are Cartesian coordinates and t is the time. We assume that a well-defined time scale T between two successive migration exists. We begin, as usual [28], noting that, between the values of time t and $t + T$, both migrations and population growth will cause a change in the number of families in an area differential $\mathrm{d}s = \mathrm{d}x\,\mathrm{d}y$, i.e.

$$[p(x, y, t + T) - p(x, y, t)]\,\mathrm{d}s = [p(x, y, t + T) - p(x, y, t)]_{\mathrm{m}}\,\mathrm{d}s + [p(x, y, t + T) - p(x, y, t)]_{\mathrm{g}}\,\mathrm{d}s, \quad (209)$$

where the subindices m and g stand for migrations and population growth, respectively.

We denote the coordinate variations of a given family during T by Δx and Δy. The effect of migrations on the evolution of $p(x, y, t)$ will be derived here by means of a simple extension of Einstein's model of Fickian diffusion [83]. The migration term in equation (209) can be written as

$$[p(x, y, t + T) - p(x, y, t)]_{\mathrm{m}}\,\mathrm{d}s = \mathrm{d}s \int_{-\infty}^{+\infty}\int_{-\infty}^{+\infty} p(x + \Delta x, y + \Delta y, t)\,\phi(\Delta x, \Delta y)\,\mathrm{d}\Delta x\,\mathrm{d}\Delta y - \mathrm{d}s\,p(x, y, t), \quad (210)$$

where $\phi(\Delta x, \Delta y)\mathrm{d}s$ is the fraction of those families lying at time t in an area $\mathrm{d}s$, centred at $(x + \Delta x, y + \Delta y)$, such that they are at time $t + T$ in an area $\mathrm{d}s$, centred at (x, y). Note that the last term in equation (210), which corresponds to the families leaving $\mathrm{d}s$, may be alternatively written as an integral, analogous to the positive term (incoming families). Both terms allow

for jumps of zero length ($\Delta x = \Delta y = 0$), but the corresponding contributions cancel out, as they should. Obviously,

$$\int_{-\infty}^{+\infty}\int_{-\infty}^{+\infty}\phi(\Delta x,\Delta y)\,\mathrm{d}\Delta x\,\mathrm{d}\Delta y = 1, \tag{211}$$

and, assuming for simplicity that the low-scale migration is isotropic,

$$\phi(\Delta x,\Delta y) = \phi(-\Delta x,\Delta y) = \phi(\Delta x,-\Delta y) = \phi(-\Delta x,-\Delta y) = \phi(\Delta y,\Delta x). \tag{212}$$

We Taylor expand the last term in equation (209),

$$[p(x,y,t+T) - p(x,y,t)]_{\mathrm{g}}\,\mathrm{d}s = \left(TF(x,y,t) + \frac{T^2}{2}\frac{\partial F(x,y,t)}{\partial t} + \cdots\right)\mathrm{d}s, \tag{213}$$

where $F(x,y,t)$ is the change, due to births and deaths, in the local population density per unit time. From equations (209), (210) and (213) we find

$$\begin{aligned} p(x,y,t+T) - p(x,y,t) = {} & \int_{-\infty}^{+\infty}\int_{-\infty}^{+\infty} p(x+\Delta x, y+\Delta y, t)\,\phi(\Delta x,\Delta y)\,\mathrm{d}\Delta x\,\mathrm{d}\Delta y \\ & -p(x,y,t) + TF(x,y,t) + \frac{T^2}{2}\frac{\partial F(x,y,t)}{\partial t} + \cdots \end{aligned} \tag{214}$$

We now assume that T, Δx and Δy are small enough in comparison with the measured time intervals and distances ($T \ll t$, $\Delta x \ll x$ and $\Delta y \ll y$) so that both sides of equation (214) may be approximated by their second-order Taylor expansions,

$$\begin{aligned} T\frac{\partial p}{\partial t} + \frac{T^2}{2}\frac{\partial^2 p}{\partial t^2} = {} & p\int_{-\infty}^{+\infty}\int_{-\infty}^{+\infty}\phi(\Delta x,\Delta y)\,\mathrm{d}\Delta x\,\mathrm{d}\Delta y + \frac{\partial p}{\partial x}\int_{-\infty}^{+\infty}\int_{-\infty}^{+\infty}\phi(\Delta x,\Delta y)\Delta x\,\mathrm{d}\Delta x\,\mathrm{d}\Delta y \\ & + \frac{\partial p}{\partial y}\int_{-\infty}^{+\infty}\int_{-\infty}^{+\infty}\phi(\Delta x,\Delta y)\Delta y\,\mathrm{d}\Delta x\,\mathrm{d}\Delta y \\ & + \frac{\partial^2 p}{\partial x^2}\int_{-\infty}^{+\infty}\int_{-\infty}^{+\infty}\phi(\Delta x,\Delta y)\frac{\Delta x^2}{2}\,\mathrm{d}\Delta x\,\mathrm{d}\Delta y \\ & + \frac{\partial^2 p}{\partial y^2}\int_{-\infty}^{+\infty}\int_{-\infty}^{+\infty}\phi(\Delta x,\Delta y)\frac{\Delta y^2}{2}\,\mathrm{d}\Delta x\,\mathrm{d}\Delta y \\ & + \frac{\partial^2 p}{\partial x\partial y}\int_{-\infty}^{+\infty}\int_{-\infty}^{+\infty}\phi(\Delta x,\Delta y)\Delta x\Delta y\,\mathrm{d}\Delta x\,\mathrm{d}\Delta y \\ & - p + TF + \frac{T^2}{2}\frac{\partial F}{\partial t}. \end{aligned} \tag{215}$$

Making use of equations (211) and (212), this reduces to

$$\frac{\partial p}{\partial t} + \frac{T}{2}\frac{\partial^2 p}{\partial t^2} = D\left(\frac{\partial^2 p}{\partial x^2} + \frac{\partial^2 p}{\partial y^2}\right) + F + \frac{T}{2}\frac{\partial F}{\partial t}, \tag{216}$$

where we have made use of the definition

$$D = \frac{1}{4T}\int_{-\infty}^{+\infty}\int_{-\infty}^{+\infty}\phi(\Delta x,\Delta y)\Delta^2\,\mathrm{d}\Delta x\,\mathrm{d}\Delta y, \tag{217}$$

with $\Delta = \sqrt{\Delta x^2 + \Delta y^2}$.

Note that equation (216) is the HRD equation (9) in 2D, with relaxation time

$$\tau = \frac{T}{2}, \tag{218}$$

which is exactly the same as that in the very simple model in section 2.1 (equation (11)) and in the ID Dirac-delta waiting time distribution model in section 2.6 (equation (60)). This

agreement supports the validity of equation (218): although the 1D model in section 2.1 holds under a stronger assumption ('jumps' of equal length), it does correspond to the case of isotropic jumps here assumed (whereas e.g. the model in section 2.2 does not). This point is extremely important because, as it will seen below, having the correct microscopic expression for τ (equation (218) in this application) is absolutely necessary in order to compare to experimental observations. This is why the derivation of the HRD equation above, which is additional to those in section 2, is indeed needed for the system under consideration in this section. The former derivation of the HRD equation, in contrast, for example, to those in sections 2.3 and 2.4, makes it also possible to note that in the application we are dealing with, the interpretation of τ is completely different from that in a reacting-diffusing gas mixture (where collisions have a negligible duration in comparison with the travel time between two subsequent collisions). The time interval T between two successive migrations is the sum of the time of travel (which may be of the order of some days or weeks) and the time of 'residence', i.e. the time interval between the arrival of a family and the subsequent migration (presumably of about one generation [84]). Therefore, in our case T is approximately the time of residence.

We will assume that the population growth can be described by

$$F = ap\left(1 - \frac{p}{p_{\max}}\right), \tag{219}$$

where a is the initial growth rate and $p_{\max}$ is the saturation density. Equation (219) is the logistic growth-function (see the discussion at the beginning of section 3), and it compares favourably to a wealth of experimental results [38]. From equations (74) and (126), equation (216) with $p = p(r)$ and $r = \sqrt{x^2 + y^2}$ leads to wavefronts with asymptotic speed of propagation ($\partial^2 p/\partial x^2 + \partial^2 p/\partial y^2 = \partial^2 p/\partial r^2 + 1/r\,\partial p/\delta r \to \partial^2 p/\partial r^2$ as $r \to \infty$)

$$v = \frac{2\sqrt{D\mathrm{d}F/\mathrm{d}p|_{p=0}}}{1 + (T/2)\mathrm{d}F/\mathrm{d}p|_{p=0}} = \frac{2\sqrt{aD}}{1 + aT/2}. \tag{220}$$

This result would not change if we considered an exponential growth-function ($F \simeq ap$) in the leading edge of the front ($p \simeq 0$). In the limit $T \to 0$, equation (220) becomes

$$v_{T\to 0} = 2\sqrt{aD}, \tag{221}$$

which is the basis of the classical wave-of-advance theory of the neolithic transition in Europe [57]. By comparing to equation (220), we note that the delay time T slows down the wavefront, as it should. The microscopic delay time T is equivalent to the relaxation time $\tau = T/2$ in the macroscopic description in sections 3.3 and 3.4.

In a different context, wavefronts for the autocatalysis $A+B \to A+A$ have been studied for a reaction term of the form $F = kp(p_0 - p)$, where p is the density of A, p_0 is the total density and k is the rate constant. In this case equation (220) can be written as $v_{T\to 0}/v = 1+(T/2)kp_0$, i.e. an additional term proportional to the rate constant is predicted. Such a term has been proposed before [17], although no explicit form for it had been derived.

We return to the problem under consideration. Equation (217) may be written as

$$D = \frac{1}{4}\frac{\bar{\Delta}^2}{T}, \tag{222}$$

in fact a well-known result for 2D diffusion. Here $\bar{\Delta}^2/T$ is the mean square displacement during the time interval T that separates two successive migrations. Previous approaches did not take the factor $1/4$ in equation (222) into account but relied on the approximation [57] $D \approx \bar{\Delta}^2/T$.

The front velocity for the expansion of agriculture can be predicted from equation (220) provided that independent estimations for the values of T, a and D are available. As in [57],

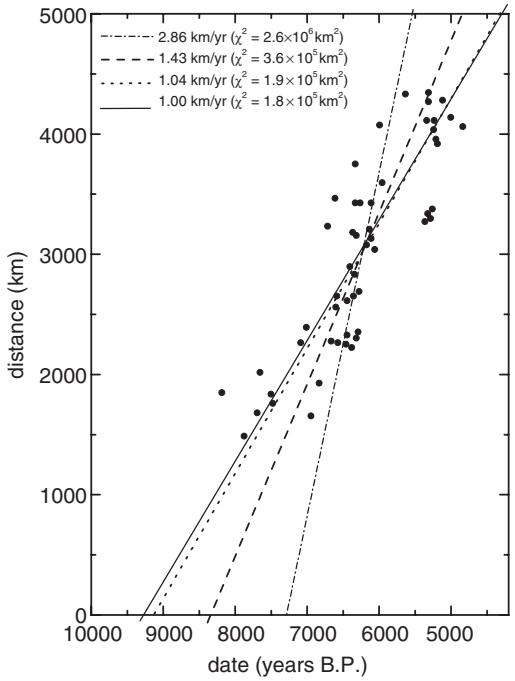

Figure 9. Comparison between empirical evidence and theoretical models for the spread of agriculture in Europe [22]. The points are the data already analysed in [57], distances being measured as great circle routes from Jericho (the presumed centre of diffusion). Dates are conventional radiocarbon ages in years Before Present. The full line is the regression by Ammerman and Cavalli–Sforza (correlation coefficient $r = 0.89$) [57]. The other three lines are least-square fits with slopes calculated from the classical wave-of-advance model with $D \approx \bar{\Delta}^2/T$ (— · —) and $D = (1/4)\bar{\Delta}^2/T$ (- - - -), and from the time-delayed model with $D = (1/4)\bar{\Delta}^2/T$ (· · · · · ·). Here $\tau = 25\,\mathrm{yr}$, $a = 0.03\,\mathrm{yr}^{-1}$ and $\bar{\Delta}^2/T = 1700\,\mathrm{km}^2$ per generation.

we consider twenty-five years for the average generation, $T = 25\,\mathrm{yr}$. Let us, for the moment, assume an initial growth rate of 3%, i.e. $a = 0.03\,\mathrm{yr}^{-1}$ [82] and $\bar{\Delta}^2/T = 1700\,\mathrm{km}^2$ per generation [57].

Figure 9 reproduces the archaeological data for the spread of the neolithic transition in Europe [57]. Use of the values above into the approximation $D \approx \bar{\Delta}^2/T$ (which was applied in [57]) and equation (221) yields a front velocity of $v_{\tau\to 0} = 2.86\,\mathrm{km\,yr}^{-1}$. In contrast, equations (221) and (222) yield a velocity of $1.43\,\mathrm{km\,yr}^{-1}$. The dashed-dotted and dashed lines in figure 9 are the best fits with these slopes, respectively. The front speed implied by $D \approx \bar{\Delta}^2/T$ is much higher than that inferred from the data. The prediction from equation (222), on the other hand, shows the usefulness of the wave-of-advance theory (provided that the factor $1/4$ in equation (222) is included, which corresponds to 2D diffusion). Still, a lower front speed is clearly implied. This may also be seen from the regression (full line) in figure 9 [57, 80]: its slope yields a velocity of $1.00\,\mathrm{km\,yr}^{-1}$. When the same values for the parameters as above are introduced into equations (220) and (222), one obtains a prediction of $v = 1.04\,\mathrm{km\,yr}^{-1}$. Therefore, the prediction from equation (216) agrees very well with observations (see the values of χ^2 in figure 9).

Changing the value of the average generation leads to much the same result (e.g. we might consider $T = 28\,\mathrm{yr}$ [57] in equations (220) and (222), which yields $v = 0.95\,\mathrm{km\,yr}^{-1}$). In figures 10 and 11, the curves labelled with number 1 give the possible values of a and

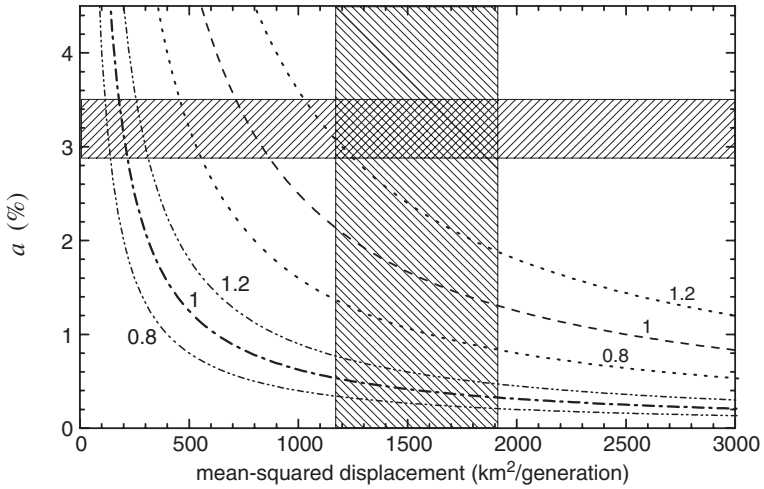

Figure 10. Predictions of the classical wave-of-advance model (equation (221)) [22]. The hatched regions correspond to the range of allowed values for a and $\bar{\Delta}^2/T$, according to the available empirical evidence. Each curve is labelled with a number, which gives the considered front velocity (in km yr^{-1}). The three lower curves correspond to the $D \approx \bar{\Delta}^2/T$ approximation, which was used in [57]. The three upper curves correspond to the same model, but taking into account equation (222) for 2D diffusion.

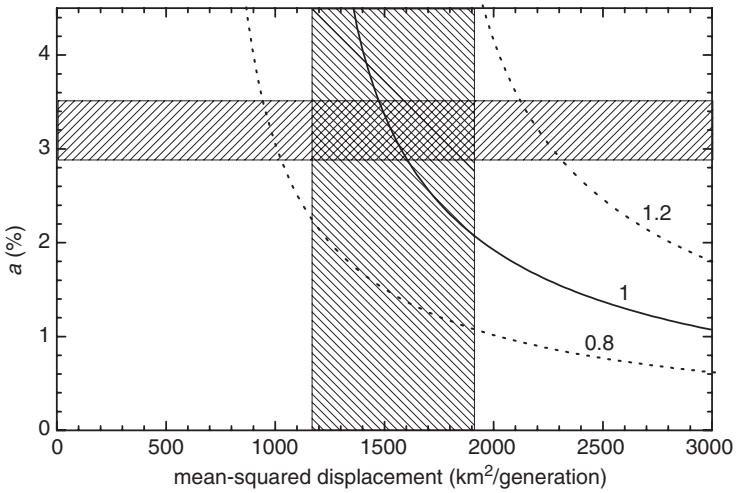

Figure 11. The same as figure 10, but for the time-delayed wave-of-advance model (equation (220)) and an average generation of $T = 25$ yr [22]. It is seen that for almost all of the likely values of the parameters a and $\bar{\Delta}^2/T$ (hatched rectangle), the predictions of the model are consistent with the observed front velocity (1.0 ± 0.2 km yr^{-1}).

$\bar{\Delta}^2/\tau$ compatible (according to each one of the three models) with the observed speed of 1 km yr^{-1}. In fact, the principal axis was preferred [81, 57] to perform a fit to the data (full line in figure 9), but the two regressions (distances versus dates and vice versa) imply a velocity range between about 0.8 and 1.2 km yr^{-1} [80]. In figures 10 and 11 we also include curves corresponding to these velocities. The hatched regions in these figures correspond to likely ranges of the parameters, and have been obtained as follows. Birdsell [85] was able to collect

detailed evolution data of two human populations which settled in empty space. A fit of these data (either to an exponential of to a logistic curve) yields $a = 0.032 \pm 0.003\,\mathrm{yr}^{-1}$, with 80% confidence-level. Values for $\bar{\Delta}^2/T$ have been derived [57, 76] from observations of Ethiopian shifting agriculturalists and Australian aborigines. A statistical analysis of these values yields $\bar{\Delta}^2/T = 1544 \pm 368\,\mathrm{km}^2$ per generation (80% C.L. interval). As we have stressed, equation (222) should replace the approximation $D \approx \bar{\Delta}^2/T$ in 2D situations. This does not rely on any assumption. From figure 10, it is seen that use of this correction (three upper curves), instead of the classical approach (lower curves), makes the non-delayed model marginally consistent with the experimental range of a and $\bar{\Delta}^2/T$ values (hatched rectangle). This shows that the first-order, or PRD, approach is compatible with the demographic data, but only assuming extreme values for the parameters. In the second-order, or HRD, model equation (220) holds, from which figure 11 follows. From this figure, we conclude that the agreement between the available empirical data and our time-delayed model is very satisfactory, in spite of the simplicity of the latter. This shows that it is not necessary to assume extreme values of the measured parameters, provided that one is willing to accept the hypothesis that a time interval T of about one generation separates successive migrations.

Finally, it is worthwhile to take into account that simulations of the neolithic transition in Europe for the values $a = 0.02\,\mathrm{yr}^{-1}$ and $\bar{\Delta}^2/T = 973.4\,\mathrm{km}^2$ per generation yield a front velocity of $v = 1.09\,\mathrm{km\,yr}^{-1}$ [76]. Making use of equation (221), the *two-dimensional* result (222) and the above values for a and $\bar{\Delta}^2/T$, we obtain $v_{T\to 0} = 0.88\,\mathrm{km\,yr}^{-1}$. In fact, in [76] an irregular lattice was considered. Since equation (222) can be easily generalized into $D = (1/2n)(\bar{\Delta}^2/T)$, where n is the number of dimensions and $2n$ is the number of neighbours in a simulation lattice, we note that a decrease in the number of neighbors corresponds to an enhancement of diffusion, as it was to be expected intuitively. If we take into account that for the irregular lattice used in [76] the mean number of neighbors was 3.4, making use of equation (221) we estimate $v_{T\to 0} = 0.96\,\mathrm{km\,yr}^{-1}$, which is closer to the value $1.09\,\mathrm{km\,yr}^{-1}$ observed in simulations. Since the simulations in [76] included corrections due to the acculturation of hunter-gatherers by farmers (which leads to a more rapid agricultural expansion, as it will be shown in section 7.1), we conclude that there is reasonable agreement between our results and the simulations. Of course, the more general result (220) cannot be compared to those in [76], simply because that study is based on equation (216) in the limit $T \to 0$.

6.2. Other population invasions

For the neolithic transition in Oceania, there are also enough archaeological data so that a front speed can be inferred [24]. The theory in the previous subsection assumes a continuous description, in the sense that all areas of 2D space are equally suitable in principle for the settlement of human populations. This may be an adequate approximation to a large-scale, space-averaged description of the observed clustered distribution of sites. A continuous description does not mean that all land areas are occupied by individuals: this is obviously impossible for small enough scales, whatever the habitat and biological population one wishes to consider. From this perspective, it is reasonable to try to apply the same model to island expansions: in this case, settlements cluster on islands, whereas large sea areas are unsettled; similarly, in mainland expansions settlements are also clustered near aquifer resources, whereas large forest areas remain unsettled. However, the diffusion coefficient has now a different value, which can again be inferred from anthropological observations, leading to good agreement with the observed speed of about $5\,\mathrm{km\,yr}^{-1}$ [24], which is much faster than that for the neolithic transition in Europe discussed in the previous subsection.

Another application refers to mass-extinctions. Simulations using PRD models ($T \to 0$) and realistic parameter values for the diffusion of hunter-gatherers predict that it took humans about $\Delta t_{T\to 0} = 1200\,\mathrm{yr}$ to colonize North-America, leading to the extinction of some 30 species of hervibores [86]. This is essentially consistent with archaeological evidence. However, this approach neglects the delay time in the diffusion process. In the approximate, single-species description above, we have from equations (220) and (221),

$$\frac{\Delta t}{\Delta t_{T\to 0}} = \frac{v_{T\to 0}}{v} = 1 + a\frac{\tau}{2}, \tag{223}$$

which using, as a first approximation, the same parameter values as above, yields about 1700 yr, i.e. a correction of about 40% relative to the PRD value. Certainly, this topic deserves further attention, both by means of time-delayed simulations which would generalize those in [86] and by means of more accurate, several-species models such as those considered in section 6. It is true, however, that if the diffusion effects dominate over the interaction among species, several-species models may yield low corrections to the single-species one (several-species models have been already applied to different process, see section 7.1).

Application of the time-delayed approach seems of utmost importance for future progress in the topic of population invasions. In the near future, it seems likely that models in the line of those reviewed will be compared to observations for different biological species. We have also explained in section 5 that such models may be also relevant to a variety of physical applications, such as combustion and solidification fronts and forest fires, for which direct comparison to experiment has yet to be performed.

7. Comparison to experiment: several-species models

7.1. Time-delayed diffusion: application to the neolithic transition

The theoretical results for interacting species (section 5) can be applied to the waves of advance of farming populations in the Indo-European neolithic transition. This problem has been considered in section 6.1 above, but without taking into account the interaction between the expanding farmers and the preexisting hunter-gatherers. This interaction is important, as mentioned in section 5, because it is thought to have caused the genetic clines (or gradients) observed in human populations across Europe and Asia [57]. This is why two-species models have been proposed for this expansion. They have been applied by means of numerical simulations [57,76] and, more recently, by an analytical approach ([43], section 5.2). Recalling that in section 3 we have introduced dimensionless variables, the speed of the front v is related to the dimensionless speed c through equation (74), $v = \sqrt{Dk}c$. We also recall that in section 5 we have introduced $a = \tau k$, $f(n) = F(n)/k$ and $\tilde{\gamma} = \gamma/k$. From equation (204) we have two cases for interacting populations:

(i) *PRD approach*: it is based on the assumption that the role of the relaxation (or delay) time can be neglected ($\tau \approx 0$). Then we have from equation (205)

$$v_{\mathrm{PRD}} = 2\sqrt{D(F'(0) + \gamma m_0)}, \tag{224}$$

which becomes Fisher's result $2\sqrt{DF'(0)}$ for noninteracting species, as it should.

(ii) *HRD approach*: it takes the delay time τ into account. Then equation (204) applies,

$$v_{\mathrm{HRD}} = \frac{2\sqrt{D(F'(0) + \gamma m_0)}}{\sqrt{(1 + \tau F'(0))^2 + 4\tau\gamma m_0}}. \tag{225}$$

In spite of the fact that the neolithic transition took place in 2D, our 1D results are still valid. This can be seen from the fact that in 2D, the only change in equations (186) is that we have $\nabla^2 n$ instead of n_{xx} (and $\nabla^2 m$ instead of m_{xx}). However, in polar coordinates $\nabla^2 n = \partial^2/\partial r^2 + 1/r\ \partial n/\partial r \to \partial^2/\partial r^2$ as $r \to \infty$, which corresponds to the asymptotic front (see p 281 in [28]): it is the propagation of this front that we are interested in (we have assumed, as usual, that n is independent of the polar angle θ).

In order to obtain numerical predictions for both speeds (224) and (225), we need values for the parameters appropriate to the neolithic transition. As explained in section 6.1, such values have been derived from observations independent of the neolithic expansion and their mean values are $F'(0) = 0.032\ \mathrm{yr}^{-1}$, $D = 15.44\ \mathrm{km}^2\ \mathrm{yr}^{-1}$ and $\tau = T/2 = 12.5\ \mathrm{yr}$ (the latter value follows from the mean generation time $T = 25\ \mathrm{yr}$). On the other hand, from the observations in [76] we have the mean values for the other two parameters $m_0 = 0.04\ \mathrm{hunters\ km}^{-1}$ and $\gamma = 5.84\ \mathrm{km}^2\ \mathrm{hunter}^{-1}\ \mathrm{yr}^{-1}$ [4]. Use of these values into equation (224) yields $v_{\mathrm{PRD}} = 1.6\ \mathrm{km\ yr}^{-1}$, which is much higher than the speed derived from the archaeological record; in contrast equation (225) yields $v_{\mathrm{HRD}} = 1.1\ \mathrm{km\ yr}^{-1}$, which lies entirely within the experimental range, namely $1.0 \pm 0.2\ \mathrm{km\ yr}^{-1}$ (see section 6.1 as well as figure 9).

As reviewed in section 6.1, when the interaction among populations is not taken into account, an HRD approach gives better results for the neolithic transition that the usual, PRD approach. The work summarized here shows that his conclusion remains valid if the effect of the interaction among farmers and hunter-gatherers is not neglected.

7.2. Replication and spread of viruses in growing plaques

In this section we review a multiple-species model of HRD equations that has been used to describe virus infections [25]. The space-time dynamics of virus populations in a growing plaque can be modelled by considering the interactions among three species, namely free viruses (V), host bacteria (B) and infected host bacteria (I). These interactions can be summarized by the reactions:

$$V + B \xrightarrow{k_1} I \xrightarrow{k_2} YV \tag{226}$$

where k_1 is the rate constant of adsorption of the viruses to the host bacteria, k_2 is the rate constant for death (or lysis) of infected bacteria, and Y is the production (or yield) of new viruses per lysed host. We focus on the relevant factors by excluding, as usual, negligible reactions such as virus desorption and their adsorption to infected hosts. The growth regions of infected bacteria (also called plaques) will not be determined only by the reactions above, since viruses must diffuse before reaching the uninfected bacteria. Let us model the process by means of the set of differential equations:

$$\begin{aligned}
\frac{T}{2}\partial_{tt}V + \partial_t V &= D_{\mathrm{eff}}\partial_{rr}V - k_1\left[VB + \frac{T}{2}\partial_t(VB)\right] \\
&\quad + Yk_2\left[\left(I\left(1 - \frac{I}{I_{\max}}\right)\right) + \frac{T}{2}\partial_t\left\{I\left(1 - \frac{I}{I_{\max}}\right)\right\}\right], \\
\partial_t B &= -k_1 VB, \\
\partial_t I &= k_1 VB - k_2 I\left(1 - \frac{I}{I_{\max}}\right),
\end{aligned} \tag{227}$$

[4] Note the units used in [76]: $\gamma = 0.002\,4$ (tribe area)/(hunter generation) $\cdot$ $(156\ \mathrm{km})^2$/(tribe area) $\cdot$ 1generation/25 yr $= 0.23\ \mathrm{km}^2\ \mathrm{hunter}^{-1}\ \mathrm{yr}^{-1}$.

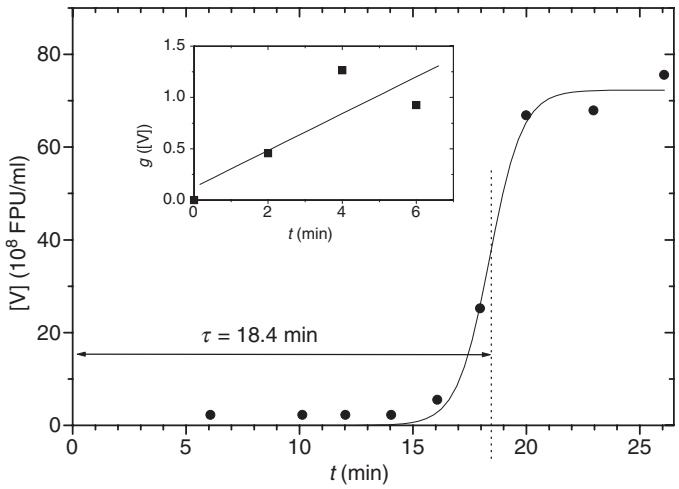

Figure 12. One-step growth curve of virus T7 on *E. coli* [25]. This experiment corresponds to an homogeneous medium ($\partial_{rr} V \approx 0$) and negligible adsorption ($\partial_t B \approx 0$) attained by dilution, so that equations (227) become $\mathrm{d}I/\mathrm{d}t = -k_2 I(1 - I/I_{\max}) = -\mathrm{d}(V/Y)/\mathrm{d}t$. The solution for V is a logistic curve, namely, $V = YI_{\max}/(1 + \exp[-k_2(t - T)])$. Full line: least-square fit of the experimental data points [92] to this equation. The full line has values $k_2 = 1.39\,\mathrm{min}^{-1}$ and $T = 18.4$ min. Inset: T7 adsorption on *E. coli*, based on the data in [90]. The assay was carried out in the presence of KCN, which is known to inhibit the phage reproduction during the time of adsorption. In such conditions, equations (227) read $\mathrm{d}V/\mathrm{d}t = -k_1 VB = \mathrm{d}B/\mathrm{d}t$ thus $B = V + \mathrm{const}$. From the initial concentrations and multiplicity in [90], we find $\mathrm{const} = 1.39 \times 10^8\,\mathrm{ml}^{-1}$. The solution for V satisfies $g(V) = \ln((V + \mathrm{const})/V) - \ln((V_0 + \mathrm{const})/V_0) = \mathrm{const}\, k_1 t$. Full line: least-square fit of the experimental data [90] to this equation. The slope yields $k_1 = (1.29 \pm 0.59) \times 10^9\,\mathrm{ml\,min}^{-1}$.

where D_{eff} is the effective diffusion coefficient and $I_{\max}$ is the saturation density of host cells. The terms in equation (227) containing $I_{\max}$ are necessary to describe—as an special case—the so-called one-step logistic growth (figure 12), which will in turn allow us to determine the value of k_2. In the first of equations (227), T is the mean time between successive jumps, here the mean time interval from the adsorption of a virus by an uninfected host and the death of the thus infected cell (it is known experimentally that when this process is completed, the virus progeny leave the cell). The time-delayed model (227) can be easily derived, for example, from a microscopic description based on a Poisson process; then, the hyperbolic model is not approximate but exact and the macroscopic relaxation time is $\tau = T/2$ (see section 2.5). Note that the first of equations (227), and the interpretation of the delay time above, is analogous to equation (216) used in the single-species, time-delayed theory of the neolithic transition in Europe, where T is the time interval between two successive migrations (section 6.1). If the delay time were neglected ($T = 0$) equations (227) would essentially reduce to the classical model of virus replication-diffusion in plaques [87–89]. Let B_0 stand for the initial concentration of bacteria, previous to the arrival of viruses. We introduce the dimensionless variables $\bar{B} \equiv B/B_0$, $\bar{V} \equiv V/B_0$, $\bar{I} \equiv I/B_0$, $\bar{t} \equiv k_2 t$, $\bar{T} \equiv k_2 T$, $\bar{r} \equiv r\sqrt{k_2/D_{\mathrm{eff}}}$, and $\kappa_1 \equiv k_1 B_0/k_2$. As explained in section 3, we look for front solutions by assuming the concentrations depend only on $\bar{z} \equiv \bar{r} - \bar{c}\bar{t}$, where $\bar{c} \equiv c/\sqrt{D_{\mathrm{eff}} k_2}$ and c is the front speed, and linearizing the system (227) in the wavefront edge $\bar{z} \to \infty$, $(\bar{V}, \bar{B}, \bar{I}) = (\varepsilon_V, 1 - \varepsilon_B, \varepsilon_I) \approx (0, 1, 0)$, with $\varepsilon = \varepsilon_0 \mathrm{e}^{-\lambda \bar{z}}$. For a solution $(\varepsilon_V, \varepsilon_B, \varepsilon_I) \neq (0, 0, 0)$ to exist, the determinant of the matrix corresponding to the linearized form of equations (227) must vanish. This yields the characteristic equation for our problem,

namely

$$\bar{c}\lambda^3\left(-1+\frac{\bar{T}}{2}\bar{c}^2\right)+\lambda^2\left\{-1+\left[1+\frac{\bar{T}}{2}(\kappa_1+1)\right]\bar{c}^2\right\}+\lambda\bar{c}\left\{1+\kappa_1\left[1-\frac{\bar{T}}{2}(Y-1)\right]\right\}=0. \tag{228}$$

If the values of the parameters are known, this equation can be solved numerically in order to find out the dimensionless front speed $\bar{c}$. This is the minimum value of $\bar{c}$ such that there exists a stable front (i.e. such that there all three roots for λ are real, and at least one of them is positive). From the one-step growth curve of virus T7 on *E. coli* host cells (figure 12), we obtain a yield of $Y = 34.5$, (the first few dots in figure 12 refer to infected bacteria [124]), a lysis rate constant of $k_2 = 1.39\,\mathrm{min}^{-1}$ and a latent period of $T = 18.4\,\mathrm{min}$. The adsorption rate constant k_1 for T7 is not so well-known and has been sometimes approximated to that of the T1 strain [88]. In fact, there are some experimental data for T7 available [90], from which we estimate k_1 to be in the range from 0.70×10^{-9} to $1.88\times10^{-9}\,\mathrm{ml\,min}^{-1}$ (figure 12, inset).The value of k_1 is thus rather uncertain. However, we will see below (especially in figure 13) that, for a wide interval of bacterial concentrations, the predictions are essentially the same throughout this range of values for k_1. The effective diffusion coefficient for a solute (viruses in our case) dispersing through a continuous medium (agar in our system) in the presence of a suspension of spheroids (host bacteria) which adsorb the solute is given by Fricke's equation [91],

$$D_{\mathrm{eff}} = D\frac{1-f}{1+f/x}, \tag{229}$$

where $f \equiv B_0/B_{\max}$ is the concentration of bacteria relative to its maximum possible value. In the experiments [88, 92, 93], f was measured indirectly by noting that the bacterial concentration B_0 (and thus $B_{\max}$) depends on the initial nutrient concentration, and typical bacterial concentrations were estimated in the range 10^7–$10^8\,\mathrm{ml}^{-1}$ [88]. In equation (229), D is the diffusion coefficient in the absence of suspended particles, and x takes care of their shape according to

$$x = \frac{-1}{1-\frac{1}{3}\left(\frac{2}{1-M/2}+\frac{1}{M}\right)}, \tag{230}$$

where

$$M = \frac{1}{\sin^2\phi'} - \frac{1}{2}\frac{\cos^2\phi'}{\sin^3\phi'}\ln\left(\frac{1+\sin\phi'}{1-\sin\phi'}\right) \tag{231}$$

and $\cos\phi' = b/a$ with a the dimension of the suspended spheroids (cells) along their axis of symmetry and b their size along the other axis. Fricke's results have been found to agree very well with experimental observations of blood cell suspensions [91, 94]. For *E. coli*, $a/b \approx 4.0$ [95], which yields $x = 1.67$. Also in equation (229) D is the diffusion coefficient of the virus through agar in the absence of bacteria, which can be approximated to that of P22 [88] because it is very similar to T7 in size and shape [96], $D = 4\times10^{-8}\,\mathrm{cm}^2\,\mathrm{s}^{-1}$ [97]. This completes the estimations of the values for all the parameters in the model from independent experiments. Now one may compare the predictions both from the time-delayed model ($T = 18.4\,\mathrm{min}$) and from the classical one ($T = 0$) to the observed infection speeds as a function of the relative bacterial concentration f, without making use of any free parameter.

In figure 13 we compare the predictions to the experimental values. The classical approach (upper curves in figures 13(*a*) and (*b*)) predicts speeds that are clearly inconsistent with the observed ones, as noted in the literature [87, 88], specially for high host concentrations

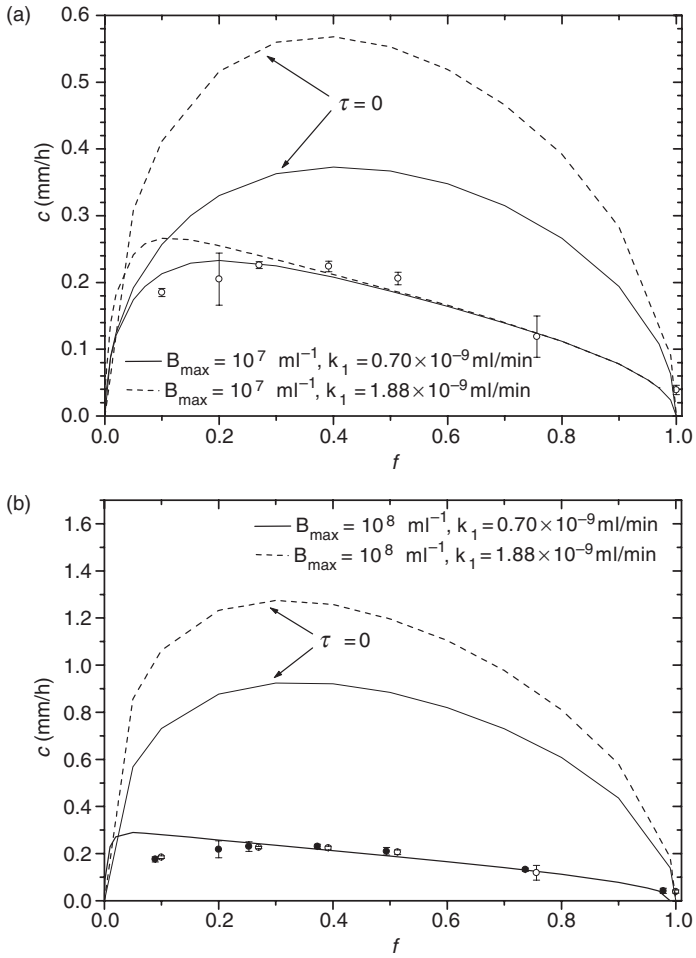

Figure 13. (*a*) Speed of the growth of virus plaques as a function of the bacterial relative concentration f [25]. Upper curves, predictions of the classical model [88], i.e. equations (227) in the present paper with $T = 0$. Lower curves, time-delayed model ($T = 18.4$ min, from figure 12). Symbols: experimental data [88]. The open and closed data symbols refer to initial bacterial concentrations of 10^7 and 10^8 ml^{-1}, respectively. The mean value and error for $f = 0.2$ has been computed by taking into account that there are some additional experimental data available for $f = 0.2$ in [92, 93]. (*b*) The two lower curves are not distinguishable from each other at this scale, showing that the uncertainty in the value of k_1 (figure 12, inset) has very little effect on the predicted speed. It is seen that the time-delayed approach is able to explain the experimental results without making use of any free parameter.

(figure 13(*b*)). In contrast, the time-delayed model (lower curves in figure 13) yields good quantitative agreement with the observations [25].

It is worth to stress that, contrary to conventional wisdom, agreement to experiment does not need to incorporate biological factors such as host aging [88] but can be attained by a purely physical model if proper care is taken of the diffusion delay time (T in equations (227)), which is a well-known physical effect [5]. Intuitively, we can understand the behaviour of the infection speed as follows. Consider first low values of the relative bacterial concentration f. The higher the value of f, the more viruses will be adsorbed by cells per unit time. This is

why the front speed increases for moderate values of f (left side of figures 13(a) and (b)). Here, the propagation of the front is reaction-controlled. This behaviour can only continue up to some intermediate value of f, however, because if bacteria occupy a large portion of the volume, then there is little space available and the mean virus dispersion distance is diminished. This will effectively reduce the spread of viruses. For high enough bacterial concentrations, therefore, the infection speed decreases with increasing values of f (right side of figures 13(a) and (b)). This may be referred to as the diffusion-controlled regime of the virus infection propagation. This model provides a satisfactory explanation for the growth of virus plaques, which is a basic problem in biophysics. It is also important because it provides an alternative way to predict and recognize virus strains, as well as their evolution [98].

8. Comparison to experiment: other kinds of time-delayed reaction–diffusion equations

Most of this review has dealt with hyperbolic equations. In this case, time derivatives up to second order appear in the reaction–diffusion equations (see, e.g. equation (9)). The simple mathematical form of hyperbolic equations allows to derive some analytical results for the speed of fronts (section 3), so that they have attracted a lot of attention in recent years. However, in some experimental situations other kinds of time-delayed reaction–diffusion equations are necessary. Therefore, we devote this section to a brief description of such models.

8.1. Infinite-term expansion model of the neolithic transition

In some systems such as those driven by a Poisson processes (section 2.5), HRD equations provide an exact description of the system dynamics. However, in other cases (e.g. sections 1.1–1.4 and 6.1), hyperbolic equations are derived by keeping some of the terms that are neglected in classical, or parabolic, reaction–diffusion. This leaves doubt on the possible importance of the additional, neglected terms. In particular, application of such a model to human population expansions leads to corrections higher than 40% with respect to the usual, non-delayed model (see sections 6.1 and 6.2). Since this modification is very large, there is no reason *a priori* to expect that keeping only a few terms will give quantitatively trustworthy results. It is thus necessary to analyse carefully the role of all higher-order terms, and we will review this point here [23]. We will focus our attention on a specific application of the model, namely the population expansion in the European neolithic transition, in order to determine whether the conclusions in section 6 remain valid or not when additional terms are included. However, we would like to remark that the formalism we will review here is valid in general, and should be useful in the future to study other systems dealing with time-delayed approaches to reaction–diffusion.

As in section 6.1, we make use of Einstein's approach to diffusion in 2D and allow for a reactive process, but keep all higher-order terms in equation (215). This immediately yields

$$\frac{\partial p}{\partial t}+\frac{T}{2!}\frac{\partial^2 p}{\partial t^2}+\cdots=\frac{\langle\Delta x^2\rangle}{2!T}\frac{\partial^2 p}{\partial x^2}+\frac{\langle\Delta y^2\rangle}{2!T}\frac{\partial^2 p}{\partial y^2}+\frac{\langle\Delta x^4\rangle}{4!T}\frac{\partial^4 p}{\partial x^4}+\frac{\langle\Delta y^4\rangle}{4!T}\frac{\partial^4 p}{\partial y^4}$$
$$+6\frac{\langle\Delta x^2\Delta y^2\rangle}{4!T}\frac{\partial^4 p}{\partial x^2\partial y^2}+\cdots+F(p)+\frac{T}{2!}\frac{\partial F(p)}{\partial t}+\cdots. \tag{232}$$

In the application considered here, $p(x, y, t)$ is the density of families per unit area at point (x, y) and time t, T is the time scale between two subsequent migrations, $\langle\Delta x^2\rangle$ is the mean square displacement in the x-direction during T, etc. The first series in the right-hand side of equation (232) is due to the diffusive process (migrations). The last series corresponds to the reactive process, i.e. population growth. We further simplify the model

by assuming that all families move a distance $\pm\Delta x$ in the x- and y-directions during T. Then $\langle\Delta x^k\rangle = \Delta x^k = \langle\Delta y^k\rangle$ for $k = 2, 4$, etc. Such lattice models are widely used in biological applications [99, 28]. Without such an approximation, comparison to observations would require the estimation of an infinite set of parameters. We introduce the diffusion coefficient as $D = \Delta^2/4T$ [99], where $\Delta^2 = \Delta x^2 + \Delta y^2 = 2\Delta x^2$ is the square displacement between subsequent migrations. Then, the only parameters in the diffusion series in equation (232) are D and T.

In the lowest-order approximation, only terms of order T^0 are kept in equation (232) and we recover Fisher's equation, namely $\partial p/\partial t = D(\partial^2 p/\partial x^2 + \partial^2 p/\partial y^2) + F(p)$. This in turn reduces, for $F(p) = 0$, to Einstein's result for diffusion [83].

Simple calculations are possible if we assume that, when a sufficiently long time has elapsed from the onset of agriculture, the farmers' wave of advance is approximately planar at scales much larger than that of individual migrations. We may then choose the x-axis parallel to the local velocity of the wave. Let $v = |v_x|$ stand for its speed ($v_y = 0$). We introduce the variable $z = x - vt$ and look for constant-shape solutions, i.e. such that p depends only on z. In general we have $F(p) = ap + b^2p^2 + \cdots$, but the migration waves of advance under consideration travel into extremely underpopulated areas, so that $F(p) \approx ap$. It is now easy to rewrite equation (232) as a differential equation involving only derivatives of p with respect to z. Wavefronts corresponding to expanding populations can be expressed as linear combinations of functions of the form $p = \exp[\lambda z]$, with $\lambda < 0$ (see section 3.1). Use of this form for p yields

$$\sum_{n=0}^{N} \frac{(-Tv\lambda)^{n+1}}{(n+1)!T} = \sum_{n=0}^{N} \frac{(2DT\lambda^2)^{n+1}}{(2(n+1))!T} + a\sum_{n=0}^{N} \frac{(-Tv\lambda)^n}{(n+1)!}, \tag{233}$$

where N denotes the order of approximation. In the lowest approximation, it is clear that the requirement $\lambda < 0$ (see section 3.1.1) imposes a minimum velocity of $v^{(0)} = 2\sqrt{aD}$, which is the Fisher–KPP result (221). In order to compare to the empirical evidence, let us assume (as in sections 6.1 and 7.1) that the time interval T between two subsequent migrations is of about one generation, $T = 25\,\mathrm{yr}$ [57, 84], and recall that available measurements of the growth [85] and diffusion [57, 76] parameters yield the mean values $a = 0.032\,\mathrm{yr}^{-1}$ and $\Delta^2/\tau = 1544\,\mathrm{km}^2$ per generation, respectively. Use of these values yields $v^{(0)} = 2\sqrt{aD} = 1.41\,\mathrm{km\,yr}^{-1}$ according to the zeroth order, or Fisher approximation. In contrast, archaeological data yield a rate of spread of $1.0 \pm 0.2\,\mathrm{km\,yr}^{-1}$ [57]. Higher-order solutions to equation (233) can be estimated numerically by requiring, as above, that $\lambda < 0$. The leading results are $v^{(1)} = 1.15\,\mathrm{km\,yr}^{-1}$ ($N = 1$) and $v^{(2)} = 1.05\,\mathrm{km\,yr}^{-1}$ ($N = 2$). The solutions are seen to converge quickly (see figure 14) to a limiting value of $v^{(\infty)} = 0.98\,\mathrm{km\,yr}^{-1}$. This result can be checked by writing equation (233) (for $N \to \infty$) as

$$(\mathrm{e}^{-v\tau\lambda} - 1)\left(1 + \frac{a}{v\lambda}\right) = [\cosh(\lambda\sqrt{2D\tau}) - 1] \tag{234}$$

and solving this equation numerically.

Consistency with the classical results can be again checked by noting that equation (232) has been obtained by dividing the ∞-term generalization of equation (215) by T. Accordingly, if we divide equation (234) by T and consider the limit $T \to 0$ we recover Fisher's dispersion relation (i.e. equation (77) with $\tau \to 0$), as it should be.

Although equation (234) cannot be solved analytically, we can show that it leads to wavefronts with a finite minimum velocity of propagation. In order to see this, in figure 15 we plot the functions in the left- and right-hand sides of equation (234). For given values of λ, D and T, the RHS has the shape shown in the figure. Then, to each possible value of the reaction (or growth) parameter a there will correspond a minimum possible value of the

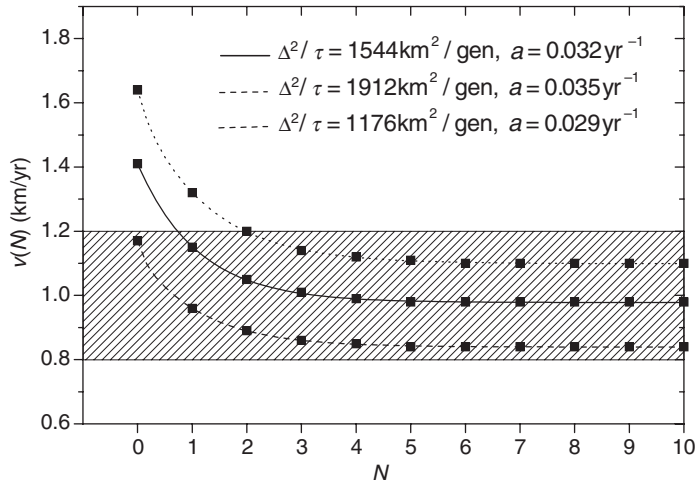

Figure 14. Predictions for the speed of spread of agriculture, as a function of the highest-order terms included in equation (233). $N = 0$ corresponds to the classical, Fisher model. Squares give the predicted speed, which has been computed for several values of the parameters Δ^2/τ and a. A statistical analysis of measurements [57, 76, 85] yields $\Delta^2/\tau = 1544 \pm 368\,\text{km}^2$ per generation and $a = 0.032 \pm 0.003\,\text{yr}^{-1}$ (80% confidence-level intervals). Results have been computed for a generation time of $\tau = 25\,\text{yr}$ [57]. The full line corresponds to mean values of the parameters, whereas the dotted and dashed lines refer to extreme values. It is seen that for $N \geqslant 2$ there is good agreement, in all cases, between the predictions of the finite-order models, the exact model and the experimentally measured range for the speed of the agricultural expansion in Europe (shaded region).

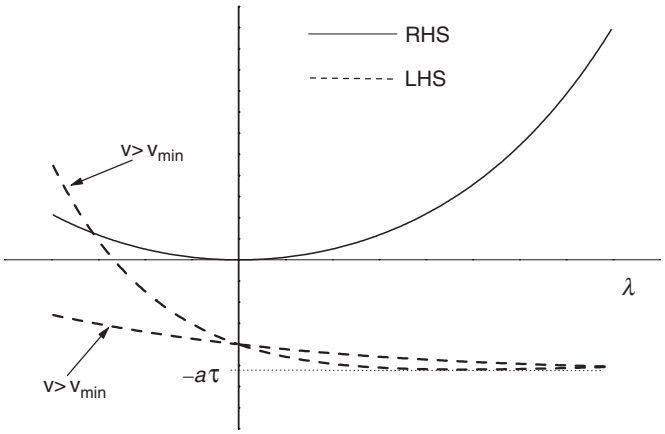

Figure 15. Plot of the left- and right-hand sides of equation (234). It is seen that a solution to this equation exists provided that v is higher than a certain minimum value which will depend on the values of the diffusive and reactive parameters D, τ and a.

velocity v, since the requirement $\lambda < 0$ implies that the LHS of equation (234) increases with increasing v: the functions in the LHS and RHS will certainly not cross for low enough values of v. Thus for given values of the parameters, a real solution to equation (234) will exist only for speeds above minimum value, in complete analogy to the Fisher and hyperbolic results obtained above by the same method.

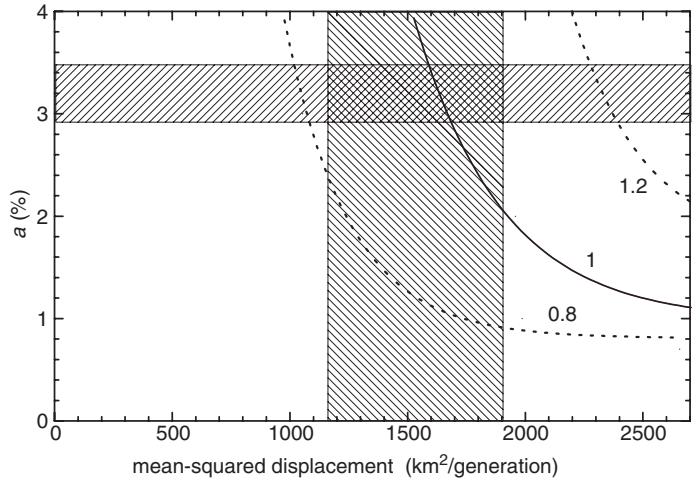

Figure 16. This figure shows the predictions of taking into account infinite higher-order terms in the mathematical model (see equation (234)). The hatched rectangle gives the values for the reaction and diffusion parameters (a and D, respectively) implied by independent observations. The curves give the values of a and D for wavefront velocities of 0.8, 1.0 and 1.2 km yr^{-1}, according to the model derived in the text. Since the velocity inferred from archaeology is 1.0 ± 0.2 km yr^{-1}, there is good agreement between theory and experiment. Comparing to figure 11 (which was obtained by including only some lower-order terms), it is seen that the hyperbolic approach (which leads to figure 11) is a reasonable approximation to the exact speed (this figure).

From figure 16, obtained by integrating equation (234) numerically, we see that the exact solution ($N \to \infty$) agrees well with the measured speed. In contrast, Fisher's result $v^{(0)}$ differs from that for $N \to \infty$ by about 44% (figure 14). We also note that the hyperbolic approximation, which is consistent with the measured speed (section 6.1), is similar in magnitude to the exact value (compare figure 11 (HRD approximation) to figure 16 (exact results)). In other applications, however, the HRD approach may not be a fair approximation, thus the exact theory above should be used to asses or improve the predictions from the hyperbolic approximation.

8.2. The spread of epidemics

Time-delayed reaction–diffusion has been applied to the spread of epidemics by Méndez [100], improving the classical, non-delayed model due to Noble [4].

Langer collected a series of statistics on the Black Death plague, which caused the death of about a quarter of the European human population [101]. The chronological spread of this plague across western and central Europe from the year AD 1347–1350 was mapped. From this, the front propagation speed was inferred ([101], see also section 20.2 in [28]).

Two different models have been proposed to take into account the incubation delay (also called infected-infectious period). As we will see, this assumption plays an important role in the speed of spread of epidemics, and the results have been compared to the case of the Black Death plague [100].

8.2.1. The SI model. This model consists of only two populations, infectious $I(x,t)$ and susceptible $S(x,t)$, which interact. We model the spatial dispersal of I and S by simple diffusion with the same diffusion coefficient D. We consider the transition rate from susceptible to infected to be proportional to rSI, where r is a constant parameter that measures

the transmission efficiency of the disease. This means that rS is the number of susceptible individuals who catch the disease from each infectious unit. The susceptible members who catch the disease become infected members, an intermediate stage between susceptible and infectious. After a period τ, infected members become infectious and may transmit the disease to other susceptible individuals with an efficiency r. We assume that the infectious members have a disease-induced mortality rate αI, where α^{-1} is the life expectancy. The evolution equations take the form

$$\begin{aligned} \partial_t S &= D\partial_{xx} S - rS(x,t)I(x,t), \\ \partial_t I &= D\partial_{xx} I + rS(x,t-\tau)I(x,t-\tau) - \alpha I(x,t). \end{aligned} \tag{235}$$

Introducing the dimensionless variables $I^* = I/S_0$, $S^* = S/S_0$, $t^* = rS_0 t$ and $x^* = x\sqrt{rS_0/D}$ where S_0 is a representative population, equation (235) becomes

$$\begin{aligned} \partial_t S &= \partial_{xx} S - S(x,t)I(x,t), \\ \partial_t I &= \partial_{xx} I + S(x,t-a)I(x,t-a) - \lambda I(x,t), \end{aligned} \tag{236}$$

where $a = \tau r S_0$, $\lambda = \alpha/(rS_0)$ and we have omitted asterisks for notational simplicity. We look for travelling wave solution to equation (236) by setting $z = x - ct$ where c is the constant wave speed which must be determined. Equation (236) yields the system

$$\begin{aligned} &S'' + cS' - IS = 0, \\ &I'' + cI' - \lambda I + \left(\sum_{n=0}^{\infty} \frac{(ca)^n}{n!}\frac{\mathrm{d}^n I}{\mathrm{d}z^n}\right)\left(\sum_{n=0}^{\infty} \frac{(ca)^n}{n!}\frac{\mathrm{d}^n S}{\mathrm{d}z^n}\right) = 0, \end{aligned} \tag{237}$$

where we have expanded in Taylor series the terms $S(x, t-a)$ and $I(x, t-a)$. The only homogeneous steady state is $(0, S_\infty)$ where S_∞ may be any positive real value. The problem consist in finding the vales of c such that a nonnegative solution for S and I exists and [4]

$$I(-\infty) = I(\infty) = 0 \qquad \text{and} \qquad 0 \leqslant S(-\infty) < S_\infty = S(\infty) = 1. \tag{238}$$

By linearizing the system (237) about the steady state we obtain

$$\begin{aligned} &v'' + cv' - u = 0, \\ &u'' + cu' - \lambda u + \sum_{n=0}^{\infty} \frac{(ca)^n}{n!}\frac{\mathrm{d}^n u}{\mathrm{d}z^n} = 0, \end{aligned} \tag{239}$$

where $u \equiv I$ and $v \equiv S - S_\infty$. The second equation in (239) is uncoupled from v and has the characteristic equation

$$\mu^2 + c\mu - \lambda + \mathrm{e}^{\mu ca} = 0 \tag{240}$$

which follows from assuming a solution of the form $u \sim \mathrm{e}^{\mu z}$. Since we must require that $I(z)$ cannot oscillate, we demand two real solutions for μ. In order to do this, it is necessary that the restriction

$$\mathrm{e}^{-c^2 a/2} < \lambda + \frac{c^2}{4} \tag{241}$$

be fulfilled.

Application to the Black Death plague. In dimensional terms, the minimum speed of travelling waves is given by $V_{\min} = 2\sqrt{rS_0 D}c_{\min}$. In order to compare the speed predicted by the model to the observed one, we must know the value of τ. This value could be related to the incubation period but a direct correspondence is not yet established. We take the same approximate values used by Noble [4]. The population density was approximately 50 persons per square miles, the diffusion coefficient was roughly obtained by estimating that news and minor gossip spread

160 km in 1 yr. Thus, D is of order $(160\,\mathrm{km})^2$ per year $\approx 10^4$ square miles per year. The transmission coefficient was $r \approx 0.4$ square miles per year and the life expectancy is about 2 weeks, so $\alpha \approx 15\,\mathrm{yr}^{-1}$. With these parameters we obtain that the classical model ($\tau = 0$) yields an asymptotic speed of 447.2 miles per year, somewhat greater than the experimental result of 200–400 miles per year. If we take the infected-infectious period of 2 weeks, which seems reasonable, the asymptotic speed predicted by the equality in (241) is 281.7 miles per year, which lies entirely in the experimental range.

8.2.2. The SII model. A second model which takes into account the infected-infectious period may be developed by including a third species [100]. Let $\hat{I}$ the number density of infected members, and I the number density of infectious members. We assume now that the infected members have an infectious transition rate $\hat{I}/\tau$, where τ is the characteristic time of transition from infected to infectious, and that all of the susceptible members who catch the disease become infected. So, the evolution equations are given by

$$\begin{aligned}
&\partial_t S = \partial_{xx} S - SI,\\
&\partial_t \hat{I} = \partial_{xx} \hat{I} + SI - \frac{\hat{I}}{a},\\
&\partial_t I = \partial_{xx} I - \lambda I + \frac{\hat{I}}{a}
\end{aligned} \tag{242}$$

in dimensionless variables. If we fix the reference frame onto the moving front by using the transformation $z = x - ct$, we get

$$\begin{aligned}
&S'' + cS' - IS = 0,\\
&\hat{I}'' + c\hat{I} - \frac{1}{a}\hat{I} + SI = 0,\\
&I'' + cI' - \lambda I + \frac{1}{a}\hat{I} = 0.
\end{aligned} \tag{243}$$

Analogously to the previous model, the homogeneous steady state is $(S, \hat{I}, I) = (1, 0, 0)$. Defining the new variables $v = S - 1$, $w = \hat{I}$, and $u = I$ and linearizing about the steady state, one obtains

$$\begin{aligned}
&v'' + cv' - u = 0,\\
&w'' + cw' - \frac{1}{a}w + u = 0,\\
&u'' + cu' - \lambda u + \frac{1}{a}w = 0.
\end{aligned} \tag{244}$$

This system of equations may be written in a compact form given by

$$\boldsymbol{U}'' + c\mathbb{I}\cdot\boldsymbol{U}' + \mathbb{A}\cdot\boldsymbol{U} = \boldsymbol{0} \tag{245}$$

where $\mathbb{I}$ is the unity matrix, $\boldsymbol{U} = (v, w, u)^{\mathrm{T}}$ and

$$\mathbb{A} = \begin{pmatrix} 0 & 0 & -1 \\ 0 & -\dfrac{1}{a} & 1 \\ 0 & \dfrac{1}{a} & -\lambda \end{pmatrix}. \tag{246}$$

By assuming a solution of the form $\boldsymbol{U} = \boldsymbol{U}_0 \mathrm{e}^{\mu z}$ we get the characteristic equation

$$\mu\left[\mu^2 + \mu\left(\lambda + \frac{1}{a}\right) + \frac{1}{a}(\lambda - 1)\right] = 0. \tag{247}$$

In order to have real values for μ, from equation (247) it is necessary that

$$c > c_{\min} = \sqrt{2}\left[\sqrt{\left(\lambda - \frac{1}{a}\right)^2 + \frac{4}{a}} - \lambda - \frac{1}{a}\right]^{1/2}, \tag{248}$$

with $\lambda < 1$.

Application to the Black Death plague. In dimensional units the asymptotic speed has the form

$$V_{\min} = \sqrt{2rS_0D}\left[\sqrt{\left(\frac{\alpha}{rS_0} - \frac{1}{\tau rS_0}\right)^2 + \frac{4}{\tau rS_0}} - \frac{\alpha}{rS_0} - \frac{1}{\tau rS_0}\right]^{1/2}. \tag{249}$$

Taking the same experimental values used in the first model we get $V_{\min} = 339.5$ miles per year which also lies in the experimental range.

Both of the two previous models use an infected-infectious delay τ of two weeks, and they lead to a speed of the disease propagation which lies entirely in the experimental range [100]. Murray [28] excuses the predictions of the classical, non-delayed approach ($\tau = 0$) on the basis that such a model is extremely simple and does not take into account the nonuniformity in population density, the stochastic processes, and so on. The fact is that, with simple extensions of the classical model based only on incorporating a time delay, substantial corrections and better results are obtained.

9. Conclusions and perspectives

In this section we first present an overview of the current status of the field reviewed, and then point out some unsolved problems and areas of likely future development.

9.1. Overview

The formulation of time-delayed equations in reactive–diffusive systems is now a topic well-advanced. Hyperbolic equations are a relevant case of time-delayed equations. They are exact in some specific systems (section 2.5) but in others they correspond to cut Taylor expansions at a finite order in the derivation of the evolution equation (e.g. sections 1.1–1.4).

The problem of wavefront speed selection for HRD equations has advanced tremendously in recent years. A wide number of techniques is now available (section 3). Depending on the system considered, the source or reactive function precludes the use of some of such methods. Thus one must choose the appropriate method of solution for each particular system. This has been applied to problems such diverse as population theory, genetic and forest fire models, bistable systems and thermal wavefronts in combustion, solidification and superconductors (section 4). The theory has been also extended to cover several-species systems, which are very important in population theory and combustion fronts (section 5).

Comparison to observations shows the usefulness of the theoretical work in several phenomena. For the neolithic transition fronts, there is substantial improvement over classical results. Here the single-species approach (section 6.1) provides a good approximation to a more detailed one incorporating several species (section 7.1). Other applications for which there are observational data available also show the importance of time-delay effects (section 6.2). A particularly appealing test of the models if provided by measurements of the front speeds for the replication and spread of viruses in growing plaques (section 7.2). Here the relevant

observational data can be easily reproduced in the laboratory. Again, time-delayed effects modify the predictions substantially, leading to good agreement with experiment.

Time-delayed models that go beyond the hyperbolic approach have also been developed in recent years. They have been already used to test the validity of the hyperbolic approach in population models (section 8.1). Moreover, they have been applied to the spread of epidemics, yielding better agreement with observational data than non-delayed models (section 8.2).

9.2. Future progress

Chemically-reacting systems [17, 18, 102, 103], superconductors [104], liquid crystals [105] and solidification [106] are topics in which extensive simulations are being performed in order to determine wavefront velocities: the methods presented here could be a useful analytical approach in situations such that the effect of a delay time could be important.

Both analytical work [17] and Montecarlo simulations [18] have predicted time-delayed effects in chemically-reacting systems similar to those here reviewed. This is an interesting topic that deserves further attention.

Another recent field of application is crystal growth and solidification fronts [19, 20] (see section 5.6). However, comparison to experiment has not yet been performed for such systems. Relevant experiments in which the speed of solidification fronts is measured [107, 108] show dendritic or needle-shape structures, which cannot be captured by means of 1D models. In view of this, numerical simulations of equations of the kind used by Galenko and Danilov [19, 20] (see equations (184) and (185)) in several dimensions could be performed in order to compare to experiment. This is similar to the fingering problem in combustion [109].

Other topics that deserve future work are combustion fronts [72] and forest fire models [73] that take proper care of the ignition delay (see section 5.6).

As far as human population expansions are concerned, here we have focused our attention in the neolithic transition in Europe simply because the quantity of archaeological observations is higher in this case than for other human expansions. We have already mentioned that for the Oceanic neolithic expansion [110], the same model also gives a good description of the process [24]. However, there is evidence that similar processes took place in Africa [111], America [112] and China [113]. The approach we have presented should in our opinion be applied to these expansions as soon as sufficient and reliable empirical data become available.

Biological population expansions are certainly a research area to which physical models should offer important contributions in the future. There are observational data available for many biological species [114–116, 125–127]. We expect that the time-delayed approaches reviewed will become widely applied in the future because of the relevant corrections they yield, as compared to non-delayed models, for the examples in which direct comparison to empirical evidence has already been performed (sections 6–8). In the long term, the final goal should be to provide a mathematical description of the temporal evolution of the geographical distribution of life on Earth. If wide time spans are to be covered, the models reviewed should be modified to incorporate the evolution of climate. This connects with another important unsolved problem, namely the mathematical description of the population range changes that are beginning to be detected because of the present climate change [117].

Concerning several-species models, an important problem that should be addressed is that of mass extinctions, for which there are experimental data available. The simple estimate in section 6.2 shows the relevance of the delay time. Several-species models as well as numerical simulations should be used to address this topic.

The spread of epidemics (section 8.2) is also a topic to which physical models which incorporate the delay time should contribute. A well-known example is the House Finch

epidemic, for which there are observational data available for the front speed, and the population growth and diffusion parameters [118]. Plant disease epidemiology is an important topic for which there are also unexplained empirical data and to which the role of the delay time has been never analysed, in spite of the importance of the latent time for most pathologies [119, 120].

Finally, we stress that the models reviewed are not restricted to a specific system and could thus be useful in the study of thermal and chemical fronts [19, 20, 17, 18, 102], plant as well as animal range expansions [121] and other biophysical topics in which reaction–diffusion is of utmost importance, such as nerve conduction [28, 58], cellular sensitivity [59], the growth of bacterial colonies [122] and models of mithocondrial tissue [123].

Acknowledgments

The authors would like to thank V Ortega-Cejas for detailed comments on a preliminary version. We also that J Farjas, A Compte, L L Cavalli–Sforza, P Roura, J Casas-Vázquez, D Jou, J E Llebot and J Camacho for discussions. Computing equipment was funded in part by the Generalitat de Catalunya under grant FGR-2001-00186 (JF and VM), and by the Ministry of Science and Technology under grants BFM-2000-0351 (JF and VM) and REN-2000-1621 CLI (JF).

References

[1] Fisher R A 1937 *Ann. Eugenics* **7** 355
[2] Zeldovich Ya B, Barenblatt G I, Librovich V B and Makhviladze G M 1985 *The Mathematical Theory of Combustion and Explosions* (New York: Consultants Bureau)
[3] Skellman J G 1951 *Biometrika* **38** 196
[4] Noble J V 1974 *Nature* **250** 726
[5] Jou D, Casas-Vázquez J and Lebon G 2001 *Extended Irreversible Thermodynamics* 3rd edn (Berlin: Springer)
[6] Maxwell J C 1867 *Phil. Trans. R. Soc.* **157** 49
[7] Cattaneo C 1948 *Atti Sem. Mat. Fis. Univ. Modena* **3** 33
[8] Vernotte P 1958 *C R Acad. Sci. Paris* **246** 3154
[9] Taylor G I 1921 *Proc. London Math. Soc.* **20** 196
[10] Ishimaru A 1978 *J. Opt. Soc. Am.* **68** 1045
[11] Neogi P 1983 *AIChE J.* **29** 829
[12] Schweizer M A 1985 *Can. J. Phys.* **63** 956
[13] Camacho J 1993 *Phys. Rev.* E **47** 1049
Camacho J 1993 *Phys. Rev.* E **48** 310
Camacho J 1993 *Phys. Rev.* E **48** 1844
[14] Fort J and Llebot J E 1998 *J. Math. Phys.* **39** 345
[15] Kac M 1974 *J. Math.* **4** 497
[16] Méndez V and Llebot J E 1997 *Phys. Rev.* E **56** 6557
[17] Gorecki J 1995 *Physica* D **84** 171
[18] Lemarchand A and Nowakowski B 1998 *J. Chem. Phys.* **109** 7028
[19] Galenko P K and Danilov D A 2000 *Phys. Lett.* A **278** 129
[20] Galenko P K and Danilov D A 2000 *J. Cryst. Growth* **216** 512
[21] Fort J, Pujol T and Cukrowski A S 2001 *J. Phys. A: Math. Gen.* **33** 6953
[22] Fort J and Méndez V 1999 *Phys. Rev. Lett.* **82** 867
[23] Fort J and Méndez V 1999 *Phys. Rev.* E **60** 5894
[24] Fort J and Cavalli-Sforza L L Wave of advance model of the Austronesian population expansion Antiquity submitted
[25] Fort J and Méndez V Time-delayed spread of viruses in a plaque submitted
[26] Horsthemke W 1999 *Phys. Lett.* A **263** 285
[27] Horsthemke W 1999 *Phys. Rev.* E **60** 2651
[28] Murray J D 1993 *Mathematical Biology* (Berlin: Springer)

[29] Kolmogorov A N, Petrovsky I G and Piskunov N S 1937 *Bull. Univ. Moscow, Ser. Int.* A **1** 1
Reprinted in Tikhomirov V M (ed) 1991 *Selected Works of Kolmogorov, A M* (Amsterdam: Kluwer)
[30] Goldstein S 1951 *Quart. J. Mech. Appl. Math.* **4** 129
Zauderer E 1989 *Partial Differential Equations of Applied Mathematics* 2nd edn (New York: Wiley)
[31] Méndez V and Camacho J 1997 *Phys. Rev.* E **55** 6476
[32] Holmes E E 1993 *Am. Nat.* **142** 779
[33] Hadeler K P 1994 *Can. Appl. Math. Quart.* **2** 27
[34] Méndez V and Fort J 1999 *Phys. Rev.* E **60** 6168
[35] Othmer H G, Dunbar S R and Alt W 1988 *J. Math. Biol.* **26** 263
[36] Dunbar S R and Othmer H G 1986 On a nonlinear hyperbolic equation describing transmission lines, cell movement, and branching random walks *Nonlinear Oscillations in Biology and Chemistry (Lecture Notes in Biomath. vol 66)* ed H G Othmer (Berlin: Springer)
[37] Hadeler K P 1999 Reaction transport systems in biological modelling *Mathematics Inspired by Biology (CIME Lectures 1997, Lecture Notes in Math. 1714)* ed V Capasso and O Diekmann (Berlin: Springer)
[38] Lotka A J 1956 *Elements of Mahtematical Biology* (New York: Dover)
[39] Aronson D G and Weinberger H F 1978 *Adv. Math.* **30** 33
[40] Dee G and Langer J S 1978 *Phys. Rev. Lett.* **50** 383
[41] Paquette G C, Chen L, Goldenfeld N and Oono Y 1994 *Phys. Rev. Lett.* **72** 76
Chen L, Goldenfeld N and Oono Y 1994 *Phys. Rev.* E **49** 4502
[42] Ben-Jacob E, Brand H R, Dee G, Kramer L and Langer J S 1985 *Physica* D **14** 348
[43] Méndez V, Fort J and Farjas J 1999 *Phys. Rev.* E **60** 5231
[44] Benguria R D, Cisternas J and Depassier M C 1995 *Phys. Rev.* E **52** 4410
[45] van Saarloos W 1988 *Phys. Rev.* A **37** 211
[46] Benguria R D and Depassier M C 1998 *Phys. Rev.* E **57** 6493
[47] Benguria R D and Depassier M C 1994 *Phys. Rev. Lett.* **73** 2272
Benguria R D and Depassier M C 1996 *Phys. Rev. Lett.* **77** 1171
Benguria R D and Depassier M C 1996 *Commun. Math. Phys.* **175** 221
[48] Gradshteyn S and Ryzhik I M 1994 *Table of Integrals, Series and Products* (San Diego: Academic)
[49] Fedotov S 1998 *Phys. Rev.* E **58** 5143
[50] Landau L D and Lifshitz E M 1960 *The Classical Theory of Fields* (Oxford: Pergamon)
[51] Fedotov S 2001 *Phys. Rev. Lett.* **86** 926
[52] Fedotov S 1999 *Phys. Rev.* E **59** 5040
[53] Fedotov S 1999 *Phys. Rev.* E **60** 4958
[54] Fedotov S 2000 *J. Phys. A: Math. Gen.* **33** 7033
[55] Méndez V and Fort J 2001 *Phys. Rev.* E **64** 011105
[56] Fort J and Méndez V 2002 *J. Stat. Phys.* **107** 805
[57] Ammerman A J and Cavalli-Sforza L L 1984 *The Neolithic Transition and the Genetics of Population in Europe* (Princeton, NJ: Princeton University Press)
[58] Engelbrecht J 1981 *Proc. R. Soc.* A **375** 195
[59] Barkai N, Rose M D and Wingeen N S 1998 *Nature* **396** 422
[60] Di Bartolo S J and Dorsey A T 1996 *Phys. Rev. Lett.* **77** 4442
[61] Wheeler A A, Boettinger W J and McFadden G B 1992 *Phys. Rev.* A **45** 7424
[62] van Saarloos W, van Hecke M and Holyst R 1995 *Phys. Rev.* E **52** 1773
[63] Press W H, Teukolsky S A, Vetterling W T and Flannery B P 1992 *Numerical Recipes* (Cambridge: Cambridge University Press)
[64] Hadeler K P and Rothe F 1975 *J. Math. Biol.* **2** 251
[65] Livshits M A, Gurija G T, Belinstev B N and Volkenstein M V 1981 *J. Math. Biol.* **11** 295
Magyari E 1982 *J.Phys. A: Math. Gen.* **15** L139
[66] Vereecken K M, Dens E J and Van Impe J F 2000 *J. Theor. Biol.* **205** 53
[67] Lieberstein H M 1967 *Math. Biosci.* **1** 45
McKean H P 1970 *Adv. Math.* **4** 209
[68] Izús G, Deza R, Ramírez O, Wio H S, Zanette D H and Borzi C 1995 *Phys. Rev.* E **52** 129
[69] Mikhailov A S 1989 *Foundations of Synergetics* vol 1 (Berlin: Springer)
[70] Landau L D and Lifshitz E M 1959 *Fluid Mechanics* (Oxford: Pergamon)
[71] Roura P, Fort J and Saurina J 2000 *Eur. J. Phys.* **21** 95
[72] Kaskiwagi T, McGrattan K B, Olson S L, Fujita O, Kikuchi M and Ito K 1996 *26th Symp. (Int.) on Combustion (The Combustion Institute, Pittsburg)* vol 1, p 1345
[73] Pyne S J 1984 *Wildland Fire* (New York: Wiley)

[74] Méndez V and Compte A 1998 *Phys. Lett.* A **260** 90
[75] Hassan S A, Kuperman M N, Wio D and Zanette D H 1994 *Physica* A **206** 380
Zanette D H 1997 *Phys. Rev.* E **55** 1181
[76] Rendine S, Piazza A and Cavalli-Sforza L L 1986 *Am. Nat.* **128** 681
[77] Dunbar S R 1983 *J. Math. Biol.* **17** 11
Dunbar S R 1984 *Trans. Am. Soc.* **268** 557
[78] Qiu T Q and Tien C L 1992 *Int. J. Heat Transfer* **35** 719
Qiu T Q and Tien C L 1993 *J. Heat Transfer* **115** 835 and 842
[79] Sobolev S L 1991 *Sov. Phys. Usp.* **34** 217
Sobolev S L and Manelis G B 1994 *Chem. Phys. Rep.* **13** 878
[80] Ammerman A J and Cavalli-Sforza L L 1971 *Man* **6** 674
[81] Diamond J M 1997 *Nature (London)* **389** 544
[82] Cavalli-Sforza L L, Menozzi P and Piazza A 1993 *Science* **259** 639
[83] Einstein A 1956 *Investigations on the Theory of the Brownian Movement* (New York: Dover)
[84] Renfrew C 1989 *Sci. Am.* **261** 87
[85] Birdsell J P 1957 *Cold Spring Harbor Symp. Quant. Biol.* **22** 47
[86] Alroy J 2001 *Science* **292** 1893
[87] You L and Yin J 1999 *J. Theor. Biol.* **200** 365–73
[88] Yin J and McCaskill J S 1992 *Biophys. J.* **61** 1540–9
[89] Fort J 2002 *J. Theor. Biol.* **214** 515
[90] Shishido K, Watarai A, Naito S and Ando T 1975 *J. Antibiot.* (Tokyo) **28** 676
[91] Fricke H 1924 *Phys. Rev.* **24** 575
[92] Yin J 1993 *J. Bacteriol.* **175** 1272
[93] Yin J 1991 *Biochem. Biophys. Res. Comm.* **174** 1009
[94] Crank J 1975 *The Mathematics of Diffusion* 2nd edn (Oxford: Oxford University Press) p 271
[95] Brock T D and Madigan M T 1991 *Biology of Microorganisms* 6th edn (Englewood Cliffs, NJ: Prentice Hall) p 40
[96] Stollar D and Levine L 1963 *Methods Enzymol.* vol VI p 848
[97] Ackermann H W 1976 *Path. Biol.* **24** 359
[98] Lee Y and Yin J 1996 *Nature Biotech.* **14** 491
[99] Okubo A 1980 *Diffusion and Ecological Problems* (Berlin: Springer)
[100] Méndez V 1998 *Phys. Rev.* E **57** 3622
[101] Langer W L 1964 *Sci. Am.* **211** 114–21
[102] Lemarchand A, Lesne A and Mareschal M 1995 *Phys. Rev.* E **51** 457
[103] Mai J, Sokolov I M and Blumen A 1996 *Phys. Rev. Lett.* **77** 4462
[104] Di Bartolo S J and Dorsey A T 1996 *Phys. Rev. Lett.* **77** 4442
[105] van Saarloos W, van Hecke M and Holyst R 1995 *Phys. Rev.* E **52** 1773
[106] Wheeler A A, Boettinger W J and McFadden G B 1992 *Phys. Rev.* A **45** 7424
Kupferman R *et al* 1992 *Phys. Rev.* B **46** 16045
[107] Herlach D M 1994 *Mater. Sci. Eng.* R **12** 177
[108] Eckler K, Kraz M and Ergy I 1993 *Rev. Sci. Instrum.* **64** 2639
[109] Zik O, Olami Z and Moses E 1998 *Phys. Rev. Lett.* **81** 3868
De Witt A 2001 *Phys. Rev. Lett.* **87** 054502
[110] Diamond J M 1988 *Nature* **336** 307
[111] Phillipson D W 1977 *The Latter Prehistory of Eastern and Southern Africa* (London: Heinemann)
[112] Moore P D 1998 *Nature* **395** 330
[113] Piazza A 1998 *Nature* **395** 636
[114] Elton C S 2000 *The Ecology of Invasions by Animals and Plants* (Chicago: University of Chicago Press)
[115] Brown J H and Lomolino M V 1998 *Biogeography* 2nd edn (Sunderland: Sinauer)
[116] Turchin P 1998 *Quantitative Analysis of Movement. Measuring and Modeling Population Redistribution in Animals and Plants* (Sunderland: Sinauer)
[117] Pounds J A, Fogden M P L and Campbell J H 1999 *Nature* **398** 611
[118] Gregory R D and Hudson P J 2000 *Nature* **406** 33
[119] Lee Campbell C and Madden L V 1990 *Introduction to Plant Disease Epidemiology* (New York: Wiley)
[120] Gilligan C A (ed) 1985 *Advances in Plant Pathology. Vol 3. Mathematical Modelling of Crop Disease* (London: Academic)
[121] Sher A 1999 *Nature* **397** 103
[122] Ben-Jacob E, Cohen I, Shochet O and Tenenbaum A 1995 *Phys. Rev. Lett.* **75** 2899

[123] Feldman A B, Chernyak Y B and Cohen R J 1998 *Phys. Rev.* E **57** 7025
[124] Delbrück M 1946 *Biol. Rev.* **21** 30
[125] Shigesada N and Kawasaki K 1997 *Biological invasions: theory and practise* (Oxford: Oxford University Press)
[126] Williamson M 1996 *Biological invasions* (London: Chapman & Hall)
[127] Hengeveld R 1989 *Dynamics of biological invasions* (London: Chapman & Hall)